# The Competition between Liquid and Vapor Transport in Transpiring Leaves[1][W][OPEN]

**Fulton Ewing Rockwell*, N. Michele Holbrook, and Abraham Duncan Stroock**

School of Chemical and Biomolecular Engineering, Cornell University, Ithaca, New York 14853 (F.E.R., A.D.S.); and Department of Organismic and Evolutionary Biology, Harvard University, Cambridge, Massachusetts 02138 (N.M.H.)

In leaves, the transpirational flux of water exits the veins as liquid and travels toward the stomata in both the vapor and liquid phases before exiting the leaf as vapor. Yet, whether most of the evaporation occurs from the vascular bundles (perivascular), from the photosynthetic mesophyll cells, or within the vicinity of the stomatal pore (peristomatal) remains in dispute. Here, a one-dimensional model of the competition between liquid and vapor transport is developed from the perspective of nonisothermal coupled heat and water molecule transport in a composite medium of airspace and cells. An analytical solution to the model is found in terms of the energy and transpirational fluxes from the leaf surfaces and the absorbed solar energy load, leading to mathematical expressions for the proportions of evaporation accounted for by the vascular, mesophyll, and epidermal regions. The distribution of evaporation in a given leaf is predicted to be variable, changing with the local environment, and to range from dominantly perivascular to dominantly peristomatal depending on internal leaf architecture, with mesophyll evaporation a subordinate component. Using mature red oak (*Quercus rubra*) trees, we show that the model can be solved for a specific instance of a transpiring leaf by combining gas-exchange data, anatomical measurements, and hydraulic experiments. We also investigate the effect of radiation load on the control of transpiration, the potential for condensation on the inside of an epidermis, and the impact of vapor transport on the hydraulic efficiency of leaf tissue outside the xylem.

During steady-state transpiration, the evaporative flux from the cell surfaces lining a leaf's intercellular airspaces balances the flux of water vapor exiting the stomatal pores. The question of how the phase change from liquid to vapor is distributed within a leaf pertains to many aspects of leaf function, including isotopic enrichment of leaf water (Farquhar et al., 1993; Gillon and Yakir, 2000; Cernusak and Kahmen, 2013), the hydromechanics of stomatal control (Buckley, 2005; Franks and Farquhar, 2007; Peak and Mott, 2011), and hydraulic constraints on maximum transpiration rates (Brodribb et al., 2007; Boyce et al., 2009; Brodribb et al., 2010). Experimental work with apoplastic tracers (Tanton and Crowdy, 1972; Byott and Sheriff, 1976), physical analogs (Meidner, 1976), and mathematical modeling (Tyree and Yianoulis, 1980; Yianoulis and Tyree, 1984) has challenged the idea that evaporation occurs more or less uniformly from the mesophyll, converging on the view that evaporation will be heavily skewed toward the internal wetted surfaces closest to the stomata (hereafter, peristomatal evaporation; Buckley and Mott, 2013). However, the interpretation of tracer accumulation as indicative of a local evaporative flux has been questioned (Yianoulis and Tyree, 1984), and calculation of the expected pressure drop for flow across the bundle sheath cells alone suggests a short liquid flow path, with evaporation from the vascular bundle directly to the airspace (hereafter, perivascular evaporation; Boyer, 1985).

At the same time, a variety of experimental approaches for characterizing the hydraulic efficiency with which leaves replace the water lost to transpiration have been developed, of which evaporative flux measurement (EFM) of transpiring leaves is considered to be the most naturalistic (Sack et al., 2002). The location and water potential of the sites of evaporation in a leaf are unknown in EFM. Instead, a whole-leaf hydraulic conductance ($K_{leaf}$) is defined as the transpirational flux ($E$) divided by the difference between the water potential of a source at the petiole (e.g. the main stem, or a reservoir in the laboratory) and leaf water potential, as typically estimated from a pressure chamber measurement (xylem sap osmolality is assumed to be negligible; Sack et al., 2002). As a result, $K_{leaf}$ is not physically well defined and bears an ambiguous relationship to the real hydraulic properties of leaf xylem and tissues (Rockwell et al., 2014b). Hydraulic studies that have sought to correlate $K_{leaf}$ with internal leaf structure have further assumed peristomatal evaporation and neglected the possibility that the phase change for some portion of the flux occurs deeper inside the leaf (Brodribb et al., 2007; Brodribb et al., 2010; Buckley et al., 2011).

[1] This work was supported by the National Science Foundation (grant no. DBI 1103664 to F.E.R.), the Air Force Office of Sponsored Research (grant no. FA9550–09–1–0188 to A.D.S. and N.M.H.), and Harvard Materials Research Science and Engineering Center (grant no. NSF DMR–0820484 to N.M.H.).

* Address correspondence to fulton.rockwell@gmail.com.

The author responsible for distribution of materials integral to the findings presented in this article in accordance with the policy described in the Instructions for Authors (www.plantphysiol.org) is: Fulton Ewing Rockwell (fulton.rockwell@gmail.com).

[W] The online version of this article contains Web-only data.

[OPEN] Articles can be viewed online without a subscription.

www.plantphysiol.org/cgi/doi/10.1104/pp.114.236323

  

Recently however, the possibility that internal vapor transport dominates liquid phase transport from the vascular bundles to a transpiring epidermis has received renewed attention, particularly in relation to stomatal behavior (Pieruschka et al., 2010; Peak and Mott, 2011). As saturated vapor pressure has a strong temperature dependence, modeling internal vapor transport requires an accounting of internal energy fluxes. In energy terms, the competition between liquid and vapor transport within a leaf can be viewed as a competition between thermal conduction and latent heat transport, as for peristomatal evaporation to occur both liquid water and thermal energy must be conducted to the transpiring epidermis. Taking a modified leaf energy balance approach, Pieruschka et al. (2010) interpreted observed stomatal opening in response to increased radiation load as evidence that latent heat transport serves as the dominant mode of energy transport from the mesophyll to the epidermis. In this model, internal vapor transport typically exceeds transpiration, with water condensing on the epidermis (peristomatal condensation) and flowing back toward the sites of short-wave energy absorption and evaporation in the mesophyll. Increasing the energy load is thought to increase condensation on the epidermis, allowing stomata to open hydropassively.

Here, we provide a model of the competition between internal liquid and vapor transport that treats the leaf mesophyll as a homogenous composite effective medium of air and cells (Rockwell et al., 2014a) and the epidermis (including stomata) as a boundary characterized by temperature, water potential, and conductance to water vapor (Fig. 1). Like Pieruschka et al. (2010), we do not attempt to model stomatal mechanics, although we will assume at some points in the analysis of steady-state transpiration a phenomenological linkage between epidermal water potential and stomatal conductance ($g_s$). The most important difference between our approach and prior work is that our model allows the competition between the vapor and liquid phase transport of water, and the associated competition between latent and sensible transport of heat energy, to emerge from general conservation laws and the constraint of local thermal and chemical equilibrium between phases in mesophyll airspaces. By contrast, Pieruschka et al. (2010) fix the balance of internal heat transport between latent transfer and heat conduction in air based on a result for steady evaporation into saturated air (equilibrium evaporation). This result says that the proportion of an absorbed solar short-wave energy load dissipated as latent heat transport assumes a characteristic value that depends only on the temperature sensitivity of saturated vapor pressure, the latent heat of vaporization, and the heat capacity of air (Raupach, 2001). Another way of expressing this result is to say that, in the absence of lateral convection (i.e. wind), the Bowen ratio (sensible heat flux/latent heat flux) for an evaporating surface assumes a value that depends only on the physical properties of water and air and not on the properties of the evaporating body itself (Bowen, 1926; Lambers et al., 1998; Raupach, 2001). It is important to note that this equilibrium evaporation result applies to a one-dimensional (1D) system of transport from water to air in series, rather than in parallel, as in the cells and airspaces of leaf mesophyll tissue.

As noted by Pieruschka et al. (2010), assuming the equilibrium evaporation result to describe energy fluxes inside a leaf affords an enormous simplification of the physical detail that must be represented in their model, yet it comes at the cost of neglecting the possibility of heat conduction in the liquid phase. As liquid phase thermal conductivity may be expected to be 1 order of magnitude larger than that of the gas phase (Tyree and

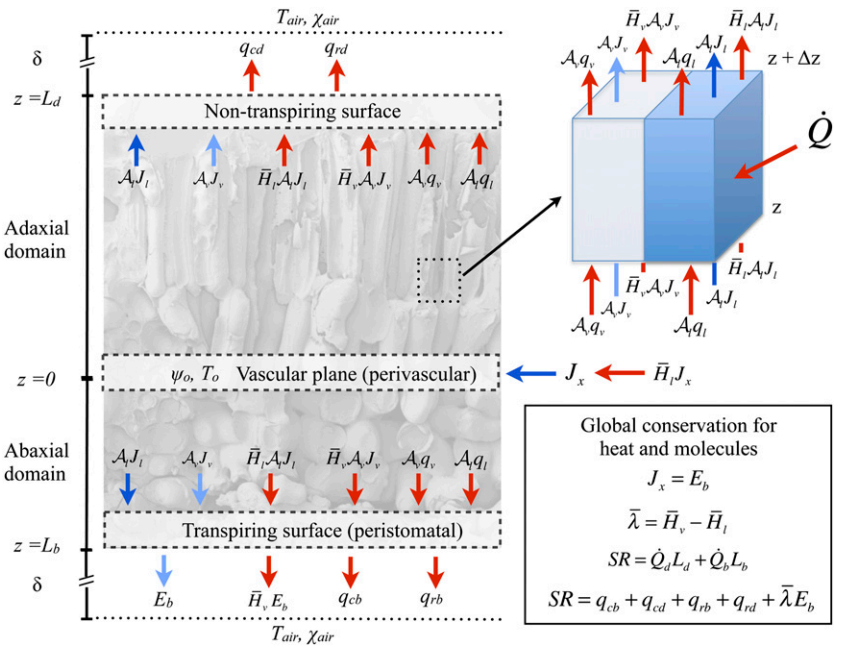


**Figure 1.** Model overview: conservation of heat and molecules at transpiring and nontranspiring surfaces and in a representative volume element of mesophyll (air and cells). At steady state, global molecular conservation requires that the number of molecules entering in the liquid phase, $J_x$, equals the number leaving in the gas phase, $E_b$, such that the difference in the enthalpies of the two phases leads to the net consumption of energy as latent heat equivalent to $\lambda E_b$. Thermal energy conservation requires that the total absorbed short-wave radiation load $SR$ balances the total net surface latent and sensible (long-wave radiative and conductive) fluxes.

Yianoulis, 1980), and as there exists continuous cell-to-cell contact through the leaf thickness in parallel with the intercellular airspaces, the actual balance of latent and sensible heat within a leaf may be quite different from the equilibrium evaporation case. Our goal, then, is to understand how the balance of vapor and liquid transport, as well as latent and sensible heat transport, depends on leaf and physical properties after relaxing the assumption that the liquid and vapor phases are arrayed in series. To do so, we account for liquid phase thermal conduction in the context of the simplest possible transport model that remains consistent with the principles of nonisothermal transport phenomena (Bird et al., 1960; Deen, 1998).

In a general way, our approach has been anticipated by effective media formulations of liquid and vapor transport in unsaturated soils, most clearly in terms of the assumption of local equilibrium between wet surfaces and the vapor in the gas-filled pores, as well as the decomposition of the mole fraction gradients driving vapor transport into gradients in temperature and water status (De Vries, 1958; Philip and De Vries, 1957; Whitaker, 1977). Our own analysis adds elements important for leaves: a volumetric energy source representing short-wave solar energy absorbed in the cells, liquid (cell) and air fractions continuously connected through the leaf thickness, a source of water at the vascular plane (Rockwell et al., 2014a, 2014b), and bounding epidermal surfaces either with or without stomata. With this approach, the combination of local equilibrium between phases and energy and mass conservation for a composite medium leads to a linkage between water potential and temperature gradients. This linkage allows us to separate the coupled equations describing heat and molecular fluxes and find analytic solutions for the temperature and water potential fields inside a leaf. We then analyze these solutions to describe the effects of leaf structural properties and surface fluxes on the distribution of evaporation between perivascular, peristomatal, and mesophyll compartments. However, the lack of a general model for the dependence of stomatal aperture on the local temperature and water potential (as well as chemical signaling) prevents us from arriving at a completely general model with which to study environmental effects. Instead, we are restricted to exploring a few cases where the $g_s$ realized for a particular set of environmental conditions is known. In the course of these analyses, we reanalyze the control of transpiration by radiation (Pieruschka et al., 2010). In exploring environmentally driven shifts in the distribution of evaporation within a particular leaf, we also clarify the relationship between $K_{leaf}$ and the actual hydraulic conductivity of leaf tissue and show that this relationship is sensitive to the energy regime experienced by a leaf. Finally, we consider the possible functional significance of the distribution of evaporation in a leaf in terms of its impact on hydraulic efficiency, the response of transpiration to environmental forcings, stomatal control, and minimum leaf water potentials.

## RESULTS

### Analytical Results

We start by providing an overview of some of the important physical ideas in our model: local thermal and chemical equilibrium in leaf airspaces, water vapor mole fraction as a function of both water potential and temperature, and the decomposition of the vapor mole fraction gradient driving the diffusion of vapor into its corresponding water potential and temperature gradients. The derivation of the model follows in Supplemental Text S1, with additional details given in Supplemental Text S2. We then analyze the model results for the distribution of evaporation between perivascular, peristomatal, and mesophyll fractions in a general way, before turning to solutions for the internal transport behavior of particular transpiring leaves for which the environmental conditions and $g_s$ could be adequately constrained.

#### *Local Equilibrium in an Unsaturated Porous Composite of Cells and Air*

We consider a representative volume of leaf tissue through the thickness composed of two domains, one upper (adaxial) and one lower (abaxial), each extending from the plane of the vasculature to an epidermis (Fig. 1) and characterized by separate area fractions for the gas phase, $A_v$ (vapor fraction), and cells, $A_l$ (liquid fraction). Within this volume of leaf tissue, we adopt the standard boundary condition of thermal and chemical equilibrium between liquid and vapor at an interface (i.e. where the cell walls contact the intercellular airspace; Deen, 1998). In the palisade mesophyll, the expectation that airspace diameters are small relative to the leaf thickness motivates the approximation that lateral gradients are negligible, limiting the analysis to the $z$ dimension. In the spongy mesophyll, airspaces can be considerably larger, yet as long as local evaporation within the spongy mesophyll is small relative to the total flux in the leaf, the extra resistance associated with lateral gradients will again be negligible. With the above conditions, we extend the interfacial boundary condition (i.e. local equilibrium between phases) across all $x,y$ planes, such that the temperature $T$ (Table I) and chemical potential of water $\mu$ describe the state of both phases and are functions of $z$ only through the entire leaf thickness. Thus, our composite medium is composed of cells and airspace in parallel, in local equilibrium at each point through the thickness (Fig. 1).

To complete the 1D model, we treat the vascular plane as a uniform (continuous, homogenous) source of water (Boyer, 1969) and the epidermal surfaces as either impermeable or characterized by a uniform $g_s$. Finally, we follow the convention in plant water relations and divide liquid phase chemical potential by the molar volume of liquid water $\overline{v}$ to define water potential, $\psi(z) = \mu(z)/\overline{v}$ (Table II).

**Table I.** *Mathematical symbols*

| Quantity | Symbol | Units[a] |
|---|---|---|
| Kelvin temperature | $T$ | K |
| Temperature, dimensionless | $\Theta$ | – |
| Water potential | $\psi$ | Pa |
| Water potential, dimensionless | $\Psi$ | – |
| Water vapor mole fraction | $\chi$ | – |
| $\partial\chi/\partial T$ | $\chi_T$ | $K^{-1}$ |
| $\partial\chi/\partial\psi$ | $\chi_\psi$ | $Pa^{-1}$ |
| Conductive heat flux | $q_c$ | J $m^{-2}$ $s^{-1}$ |
| Radiative heat flux | $q_r$ | J $m^{-2}$ $s^{-1}$ |
| Absorbed short-wave radiation per volume | $Q$ | J $m^{-3}$ $s^{-1}$ |
| Transpirational flux | $E$ | mol $m^{-2}$ $s^{-1}$ |
| Internal vapor flux | $J_v$ | mol $m^{-2}$ $s^{-1}$ |
| Internal liquid flux | $J_l$ | mol $m^{-2}$ $s^{-1}$ |
| Hydraulic conductivity, leaf | $k_\ell$ | mol $m^{-1}$ $Pa^{-1}$ $s^{-1}$ |
| Stomatal conductance | $g_s$ | mol $m^{-2}$ $s^{-1}$ |
| Boundary layer conductance | $g_{bl}$ | mol $m^{-2}$ $s^{-1}$ |
| Boundary layer thickness | $\delta$ | m |
| Emissivity, long wave | $\epsilon_{IR}$ | – |
| Absorptance, long wave | $a_{IR}$ | – |
| Absorptance, short wave | $a_{sw}$ | – |

[a]Dashes indicate a dimensionless (unitless) quantity.

### *The Dependence of Water Vapor Mole Fraction on Temperature and Water Potential*

The depression of saturated water vapor pressure above a salt solution or a curved meniscus is a familiar phenomenon in plant physiology. From a thermodynamic perspective, salts reduce the chemical potential of the liquid phase by lowering the activity of the water, while a curved meniscus acts on the pressure term of the chemical potential. A general expression that integrates all such effects can be written in terms of chemical potential, or more conveniently, water potential, as:

$$p_v(T,\psi) = p_v(T)\exp\frac{\psi\overline{v}}{RT} \quad (1)$$

where $p_v(T,\psi)$ is the vapor pressure, $p_v(T)$ is the vapor pressure above pure water at atmospheric pressure with a flat interface, $\overline{v}$ is the molar volume of water, $R$ is the ideal gas constant, and $T$ is the temperature (K; Pickard, 1981; Nobel, 2005). For gas-exchange measurements, the difference between $p_v(T,P_{atm})$ and $p_v(T,\psi)$ is typically trivial relative to the difference in vapor pressure between the leaf and the unsaturated surrounding air. For studying vapor transport inside the leaf, we will see that we must maintain the distinction.

Vapor pressure as a function of temperature $T$ (K) can be represented by the Clausius-Clapeyron equation (Whitaker, 1977; Kittel and Kroemer, 1980):

$$p_v(T) = p_{v,o}(T_o)\exp\left[-\frac{\overline{\lambda}}{R}\left(\frac{1}{T}-\frac{1}{T_o}\right)\right] \quad (2)$$

where $\overline{\lambda}$ is the latent heat of vaporization evaluated at the reference temperature $T_o$ and $p_{v,o}(T_o)$ is the reference vapor pressure when the liquid phase is at atmospheric pressure (e.g. as tabulated by Nobel [2005]). Combining Equations 1 and 2 yields an expression for vapor pressure as a function of temperature and water potential. As the appropriate driving force for nonisothermal vapor diffusion is the mole fraction of water vapor, $\chi = p_v/P_{atm}$ (Bird et al., 1960), we divide by atmospheric pressure $P_{atm}$ to arrive at an expression for the mole fraction of water vapor in local equilibrium with a liquid phase at temperature $T$ and water potential $\psi$:

$$\chi(T,\psi) = \chi_o(T_o)\exp\left[-\frac{\overline{\lambda}}{R}\left(\frac{1}{T}-\frac{1}{T_o}\right)+\frac{\psi\overline{v}}{RT}\right] \quad (3)$$

### *Description of the Fluxes of Heat and Molecules*

Fourier's law for the flux of thermal energy due to conduction $q$, with $l$ and $v$ referencing the liquid and vapor phases and $k^T$ a thermal conductivity, takes the following forms:

$$q_l = -k_l^T\frac{\partial T}{\partial z},\ q_v = -k_v^T\frac{\partial T}{\partial z} \quad (4)$$

To describe the flux of molecules in the liquid phase $J_l$, we adopt a form of Darcy's law:

$$J_l = -k_l\frac{\partial\psi}{\partial z} \quad (5)$$

where $k_l$ is the hydraulic conductivity of the cells (inclusive of the apoplast and symplast; Molz and Ferrier, 1982; Rockwell et al., 2014a).

**Table II.** *Physical quantities and constants used in the analyses*

| Quantity | Symbol | Value (25°C) | Units[a] |
|---|---|---|---|
| Latent heat, molar | $\overline{\lambda}$ | $44 \times 10^3$ | J $mol^{-1}$ |
| Molar enthalpy of water, liquid | $\overline{H}_l$ | $1.88 \times 10^3$ | J $mol^{-1}$ |
| Molar enthalpy of water, vapor | $\overline{H}_v$ | $45.88 \times 10^3$ | J $mol^{-1}$ |
| Thermal conductivity air | $k_v^T$ | 0.026 | J $m^{-1}$ $K^{-1}$ $s^{-1}$ |
| Molar volume of water, liquid | $\overline{v}$ | $1.807 \times 10^{-5}$ | $m^3$ $mol^{-1}$ |
| Diffusivity, water in air | $D_v$ | $2.5 \times 10^{-5}$ | $m^2$ $s^{-1}$ |
| Molar concentration of air | $c$ | 40.86 | mol $m^{-3}$ |
| Gas constant | $R$ | 8.3145 | J $mol^{-1}$ $K^{-1}$ |
| Stefan-Boltzmann constant | $\sigma$ | $5.67 \times 10^{-8}$ | J $m^{-2}$ $s^{-1}$ $K^{-4}$ |
| Atmospheric pressure | $P_{atm}$ | $101.3 \times 10^3$ | Pa |
| Reference temperature | $T_o$ | 298.15 | K |
| Reference vapor mole fraction | $\chi_o$ | 0.0313 | – |
| Reference vapor pressure | $p_o$ | $3.173 \times 10^3$ | Pa |

[a]Dashes indicate a dimensionless (unitless) quantity.

For nonisothermal vapor diffusion, neglecting a small amount of convection set in motion by the addition of water molecules to the gas phase (Supplemental Text S2), Fick's law for the vapor flux $J_v$ takes the form (Bird et al., 1960):

$$J_v = -cD_v \frac{\partial \chi}{\partial z} \tag{6}$$

Here, $c$ is the total number of moles of molecules in the gas phase and $D_v$ is the diffusivity of vapor in air. With Equation 3, the gradient in the water vapor mole fraction can be expressed in terms of the water potential of the liquid phase and temperature, such that Fick's law can be written:

$$J_v = -cD_v \left( \chi_\psi \frac{\partial \psi}{\partial z} + \chi_T \frac{\partial T}{\partial z} \right) \tag{7}$$

where $\chi_\psi$ and $\chi_T$ are the partial derivatives of the mole fraction of water vapor (Eq. 3) and, along with $cD_v$, are evaluated numerically at a temperature and water potential that characterizes the leaf; here, we use the temperature and water potential of the vascular plane. This linearization results in errors of less than 1% in calculating changes in vapor mole fraction over changes in temperature and water potential inside a leaf of less than 2°C and 2 MPa, respectively. While $\chi_\psi/\chi_T \sim 0.12\ \mathrm{K\,MPa^{-1}}$, given that expected internal temperature differences are on the order of 0.1°C and water potential differences are on the order of 1 MPa for leaf tissue (Yianoulis and Tyree, 1984), both temperature and water potential appear likely to have important effects on the internal water vapor mole fraction gradient in leaves (the term in brackets on the right side of Eq. 7).

### *Analysis of the Competition of Heat Conduction and Latent Transport in Leaf Tissue*

Combining conservation of thermal energy and water molecules in two phases (gas and liquid) for leaf tissue subject to a volumetric load of absorbed solar short-wave radiation, $\dot{Q}$, the description of the fluxes (Eqs. 4, 5, and 7), and local equilibrium between the liquid and gas phases (Eq. 3) leads directly to governing equations for the water potential and temperature profiles (Supplemental Text S1, Equations 1.5 and 1.7). The water potential profile is governed by a steady diffusion equation with a source (Crank, 1957):

$$0 = -\Pi_\psi \, \mathcal{A}_l \overline{\lambda} k_l \frac{\partial^2 \psi}{\partial z^2} + \dot{Q} \tag{8}$$

where $\Pi_\psi$ is a dimensionless parameter we call the thermal dissipation modulus. In words, Equation 8 says:

$$0 = \Pi_\psi \times \text{ energy into local evaporation} + \text{local energy load} \tag{9}$$

This modulus describes the tendency of internal leaf tissue toward dissipating a thermal load, $\dot{Q}$, by internal latent heat transport (dominant when $\Pi_\psi$ is close to 1) versus internal heat conduction (dominant when $\Pi_\psi$ is large). In its definition, $\Pi_\psi$ integrates all of the effects of the thermal, hydraulic, and diffusive properties of the tissue on the local evaporative process into a single parameter:

$$\Pi_\psi \equiv 1 + \frac{\mathcal{A}_l k_l^T + \mathcal{A}_v k_v^T}{\mathcal{A}_v \overline{\lambda} c D_v \chi_T} + \frac{\mathcal{A}_l k_l^T + \mathcal{A}_v k_v^T}{\mathcal{A}_l \overline{\lambda} k_l} \frac{\chi_\psi}{\chi_T} = \frac{\text{total thermal conductivity}}{\text{latent heat conductivity}} \tag{10}$$

The two ratios that appear in $\Pi_\psi$ describe total thermal conductivity over particular components of latent heat transport, and $\Pi_\psi$ is thus analogous to the Bowen ratio. The first ratio:

$$\frac{\text{total thermal conductivity}}{\text{temperature driven latent heat}} = \frac{\mathcal{A}_l k_l^T + \mathcal{A}_v k_v^T}{\mathcal{A}_v \overline{\lambda} c D_v \chi_T} \tag{11}$$

compares thermal conductivity with latent heat transport due to temperature-dependent gradients in the vapor mole fraction. The second ratio in $\Pi_\psi$:

$$\frac{\text{total thermal conduction}}{\text{local evaporation}} = \frac{\mathcal{A}_l k_l^T + \mathcal{A}_v k_v^T}{\mathcal{A}_l \overline{\lambda} k_l} \frac{\chi_\psi}{\chi_T} \tag{12}$$

compares the relative magnitudes of the heat moved by conduction versus the evaporation of a liquid flux, as driven by the temperature and water potential differences that result in equal changes in the vapor mole fraction, $\chi_\psi/\chi_T$.

As the temperature and water potential profiles are linked by both the process of evaporation and their effects on the vapor mole fraction gradients (Eq. 7), the governing equation for temperature follows the same form as for water potential (Eq. 8):

$$0 = \Pi_T \left( \mathcal{A}_l k_l^T + \mathcal{A}_v k_v^T \right) \frac{\partial^2 T}{\partial z^2} + \dot{Q} \tag{13}$$

where again the behavior depends on a second dimensionless parameter, $\Pi_T$. This equation says that a local energy load will be dissipated by thermal conduction when $\Pi_T$ approaches 1; however, there is no new information in this parameter, as they are not independent ($\Pi_\psi^{-1} + \Pi_T^{-1} = 1$), and we restrict our analysis here to $\Pi_\psi$.

The composition of $\Pi_\psi$ as two independent ratios (Eq. 10), each representing a competition between thermal conduction and an aspect of latent transport, is such that thermal conduction need only win one to serve as the dominant sink for absorbed radiation. Physically, this structure arises from the fact that within a representative volume being loaded with energy, thermal conduction and latent transport are

parallel processes, but local evaporation depends on properties of the liquid phase (cell fraction, hydraulic conductivity) and vapor phase (air fraction, diffusivity) that, with respect to a change of phase from liquid to vapor, are arrayed in series. Thus, the transport properties of either phase can independently create a bottleneck, reducing the competitiveness of local vapor production (and so latent heat transport) as a sink for the absorbed energy load.

With respect to the value of $\Pi_\psi$ expected for leaves, if the thermal conductivity of the cells is assumed to be, in general, close to that of water (Tyree and Yianoulis, 1980), with low variability between plants, then this first ratio (Eq. 11) will vary between the palisade and spongy tissues, as well as between leaves, mostly as a function of the liquid and air fractions, $A_v$ and $A_l$, as the other parameters are all material properties. On the other hand, the ratio in Equation 12 is only weakly affected by area fractions, with the hydraulic conductivity of the cells, $k_l$, likely the most important source of variation between (and possibly within) leaves. Given that pressure probe data suggest that leaf cell membrane permeability spans 2 orders of magnitude, the potential exists for this term to range from near zero to more than 10 (Kramer and Boyer, 1995; Rockwell et al., 2014a). Thus, a domain of leaf tissue might have very large air fractions, favoring latent heat transport in the first ratio, but if the hydraulic conductivity of the cells is at the low end of the expected values, it could limit vapor production to the extent that heat conduction emerges as the dominant local mode for the dissipation of absorbed radiation.

### *Analytical Results for the Distribution of Evaporation*

Evaluating $\Pi_\psi$ provides important information regarding the characteristic behavior of a representative volume of mesophyll, yet it cannot tell us the overall distribution of evaporation within a whole leaf: the environmental conditions and fluxes at the leaf surfaces are also important. Solving the governing equations (Eqs. 8 and 13) with the appropriate transpiring or nontranspiring boundary conditions at the epidermal surfaces (Supplemental Text S1, Equations 1.15, 1.16, 1.21, and 1.22) leads to general solutions for $\psi(z)$ and $T(z)$ (Supplemental Text S1, Equations 1.17, 1.18, 1.23, and 1.24). These solutions can then be analyzed to find expressions for the proportion of transpiration that originates in a mesophyll, perivascular, or peristomatal region as functions of the tissue properties and surface fluxes. We define peristomatal evaporation as the liquid flux ($-\mathcal{A}_l k_l \partial\psi/\partial z$, a positive quantity) arriving at a transpiring epidermis ($z = L$), where it consumes energy to change phase and contribute to $E$. As a proportion of transpiration from an epidermal surface, the peristomatal fraction is found by evaluating with parameter values specific to the particular domain:

$$\text{Peristomatal fraction: } -\frac{\mathcal{A}_l k_l}{E}\left.\frac{\partial\psi}{\partial z}\right|_{z=L} = -\frac{q_c + q_r}{\Pi_\psi\,\overline{\lambda}E} + \left[1 + \frac{\overline{\lambda}\mathcal{A}_v c D_v \chi_T}{\mathcal{A}_l k_l^T + \mathcal{A}_v k_v^T} + \frac{\mathcal{A}_v c D_v \chi_\psi}{\mathcal{A}_l k_l}\right]^{-1} \tag{14}$$

Here, $q_c$ is heat conduction to the surrounding air and $q_r$ is net long-wave radiation to the environment. Peristomatal evaporation has two contributions, again both analogous to Bowen ratios. The first contribution relates to the external environment:

$$\frac{\text{sensible heat flux from surface}}{\text{scaled latent heat flux from surface}} = -\frac{q_c + q_r}{\Pi_\psi\,\overline{\lambda}E} \tag{15}$$

and represents the Bowen ratio of the surface fluxes, scaled by $\Pi_\psi$ in the denominator, such that when internal thermal conduction is dominant, the effects of energy exchange with the environment are muted. The second contribution to the peristomatal fraction (in brackets) is composed of two ratios involving material properties. The inverse of the first ratio was discussed above (Eq. 11), describing the competition between temperature-driven latent heat transport and thermal conduction. The second ratio:

$$\frac{\text{vapor transport due to water potential}}{\text{liquid transport}} = \frac{\mathcal{A}_v c D_v \chi_\psi}{\mathcal{A}_l k_l} \tag{16}$$

describes the isothermal competition between liquid and vapor. Thus, the bracketed material property ratios capture the fact that for peristomatal evaporation to occur, both thermal energy and water must flow to a transpiring surface. Notably, both ratios are sensitive to the amount of airspace, making the air fraction a critical parameter for the peristomatal fraction.

It will be noted that for leaves much warmer than the surroundings, and/or when transpiration is suppressed by high humidity or stomatal closure, the entire peristomatal fraction (Eq. 14) can evaluate as negative. Physically, this describes condensation on the inner epidermal surface and flow back toward evaporating sites in the mesophyll (i.e. the internal vapor flux exceeds $E$). A test for the existence of such a condensing flux can then be derived from Equation 14 as:

$$\frac{(q_c + q_r)}{\overline{\lambda}E} > \frac{\left(\mathcal{A}_l k_l^T + \mathcal{A}_v k_v^T\right)}{\overline{\lambda}\mathcal{A}_v c D_v \chi_T} \tag{17}$$

This emphasizes that condensation occurs whenever the sensible heat transport is more important externally than internally, as this requires that some of the

internally transported latent heat become available by condensation to balance the external sensible flux.

It will also be noted that the peristomatal fraction can evaluate to more than 1. For transpiring leaves cooler than the surrounding air (as may occur in the shade or subcanopy), the sensible heat flux is negative (i.e. toward the leaf), and Equation 15 adds to the peristomatal fraction. A fraction greater than 1 corresponds physically to an evaporative flux from the inner face of the epidermis to the mesophyll. Within the mesophyll, evaporation is energy limited, and evaporation is favored near the surfaces where sensible heat from the surrounding air is warming the leaf.

The proportion of $E$ originating as evaporation within the mesophyll of either the adaxial or abaxial mesophyll is found by integrating the change in the liquid flux through the mesophyll thickness:

$$\text{Mesophyll fraction: } \frac{\mathcal{A}_l k_l}{E}\int_0^L \frac{\partial^2\psi}{\partial z^2}dz = \frac{\dot{Q}L}{\Pi_\psi \overline{\lambda} E} \qquad (18)$$

Mesophyll evaporation, then, is the sum of the local evaporation that occurs within a domain due to the total thermal load absorbed in that domain, as determined by $\Pi_\psi$. The expected behavior is that, in the palisade where the absorbed load is large (favoring a large mesophyll fraction), $\Pi_\psi$ will also tend to be large (and local evaporation will be small), as the tight packing of cells leads to a large liquid phase fraction and, therefore, efficient heat conduction. In the spongy mesophyll, airspaces tend to be more extensive, reducing the efficiency of thermal conduction and favoring local evaporation, but the locally absorbed radiation load will be much smaller (Vogelmann and Evans, 2002). Therefore, here again, total local evaporation may amount to a minor component of $E$.

The remaining fraction of $E$ originating within a single domain is perivascular evaporation. As the vapor flux from the vascular plane into, for example, the spongy mesophyll may include vapor originating in the palisade, both domains must be considered together. Total perivascular evaporation (i.e. unnormalized by $E$) for both domains can be found by evaluating the vapor fluxes into each domain (abaxial [b] and adaxial [d]) from the vascular plane:

$$\text{Perivascular fraction: } -\left[\mathcal{A}_v c D_v\left(\chi_\psi\frac{\partial\psi}{\partial z}+\chi_T\frac{\partial T}{\partial z}\right)\Big|_{z=0}\right]_b-\left[\mathcal{A}_v c D_v\left(\chi_\psi\frac{\partial\psi}{\partial z}+\chi_T\frac{\partial T}{\partial z}\right)\Big|_{z=0}\right]_d \qquad (19)$$

If both fluxes are positive (i.e. into their respective domains), then within each domain, perivascular evaporation is indeed equal to the vapor flux at that boundary. In the event that one of them is negative (i.e. out of its domain), then the sum in Equation 19 gives the perivascular vapor flux of the other (positive flux) domain. As no energy is absorbed at the vascular plane (it has infinitesimal volume), the energy to evaporate a vapor flux comes from the difference between heat conduction into the perivascular plane from the palisade versus that out into the spongy. A large difference in the cell area fraction $A_l$ between palisade and spongy creates a drop in total thermal conductivity across the perivascular plane, which then helps push energy from conduction into perivascular evaporation at the palisade-spongy boundary.

## Numerical Results

The above analysis has examined the factors influencing the distribution of evaporation in leaves in a general way. In the following, we next consider specific instances, red oak (*Quercus rubra*) and sunflower (*Helianthus annuus*), based on experimental data, as well as additional model simulations to explore particular phenomena.

### *Distribution of Evaporation in a Transpiring Red Oak Leaf*

*Solution for a Within-Cuvette Energy Balance.* We first consider transpiring red oak leaves, for which all the surface fluxes as well as $g_s$ are known. Using gas-exchange measurements (LI-6400; Li-Cor) of five upper canopy transpiring oak leaves under sunny summer conditions (Table III) with additional hydraulic and anatomical measurements on adjacent leaves, we solved the temperature and water potential profiles through the leaf thickness, both for surface energy balances within the gas-exchange cuvette and for surface energy balances for epidermal surfaces exposed to the environment. The latter solutions for the internal and external fluxes of heat and water are shown in Figure 2; as we considered the exposed leaf closer to the state of an oak leaf in nature, we chose to present those data in the figure rather than the within-cuvette results. After measurement of gas exchange, the five leaves were then collected to determine the average water potential of each leaf imposed by transpiration, $\psi_{leaf}$ (e.g. transpiring potential). This water potential provided an independent check for the within-cuvette solution as well as a required constraint for the exposed-leaf solution, made necessary because leaf absorptance and environmental reflectance were not measured directly.

The within-cuvette distribution of evaporation yielded a dominant peristomatal fraction (74.5%), with most of the balance perivascular (21.3%) and only minor contributions from evaporation in the mesophyll tissues (1.5% and 2.7%). The water potential drop from the branch (−1.29 MPa, as measured by covered leaves) to the vascular plane (−1.69) was estimated at 0.4 MPa, with the upper domain sitting close to the vascular plane water potential. A steep drop to the transpiring surface (at −2.51 MPa) put the lower epidermis close to the whole-leaf turgor loss point, as estimated from pressure volume curves measured previously for these trees (Rockwell et al., 2011).

**Table III.** *Leaf and environmental parameter values used in the various solutions reported in the figures*

| Quantity | Symbol | Red Oak (Fig. 2) | Sunflower (Fig. 3) | Condensing Leaf (Fig. 4) | EFM Leaf (Fig. 5) | Units[a] |
|---|---|---|---|---|---|---|
| Leaf thickness, adaxial | $L_d$ | $167.7 \times 10^{-6}$ | $200 \times 10^{-6}$ | $167.7 \times 10^{-6}$ | $167.7 \times 10^{-6}$ | m |
| Leaf thickness, abaxial | $L_b$ | $94.3 \times 10^{-6}$ | $200 \times 10^{-6}$ | $94.3 \times 10^{-6}$ | $94.3 \times 10^{-6}$ | m |
| Liquid area fraction, adaxial | $\mathcal{A}_{ld}$ | 0.95 | 0.8 | 0.8 | 0.8 | – |
| Liquid area fraction, abaxial | $\mathcal{A}_{lb}$ | 0.7 | 0.2 | 0.15 | 0.4 | – |
| Vapor area fraction, adaxial | $\mathcal{A}_{vd}$ | 0.05 | 0.2 | 0.2 | 0.2 | – |
| Vapor area fraction, abaxial | $\mathcal{A}_{vb}$ | 0.3 | 0.8 | 0.85 | 0.6 | – |
| Palisade absorbed radiation | $\dot{Q}_d L_d$ | 0.8 *SR* | 0.9 *SR* | 0.8 *SR* | 0.8 *SR* | J $m^{-2}$ $s^{-1}$ |
| Spongy absorbed radiation | $\dot{Q}_b L_b$ | 0.2 *SR* | 0.1 *SR* | 0.2 *SR* | 0.2 *SR* | J $m^{-2}$ $s^{-1}$ |
| Leaf hydraulic capacity | $c_\ell$ | $9.3 \times 10^{-4}$ | – | – | – | mol $m^{-3}$ $Pa^{-1}$ |
| Vascular conductance | $h_A$ | $2.1 \times 10^{-8}$ | $1 \times 10^{-7}$ | $2.1 \times 10^{-8}$ | $2.1 \times 10^{-8}$ | mol $m^{-2}$ $Pa^{-1}$ $s^{-1}$ |
| Vascular conductance scaling factor | $\varsigma$ | 0.67 | – | – | 0.6 - 0.8 | – |
| Root and stem conductance | $K_{rs}$ | – | – | $6 \times 10^{-9}$ | – | mol $m^{-2}$ $Pa^{-1}$ $s^{-1}$ |
| Hydraulic conductivity cells | $k_l$ | $6.97 \times 10^{-13}$ | $1 \times 10^{-12}$ | $6.97 \times 10^{-13}$ | $6.97 \times 10^{-13}$ | mol $m^{-1}$ $Pa^{-1}$ $s^{-1}$ |
| Thermal conductivity cells | $k_l^T$ | 0.286 | 0.2 | 0.286 | 0.286 | J $m^{-1}$ $K^{-1}$ $s^{-1}$ |
| Stomatal conductance, total | $g_s$ | 0.3 | 0.71 | 0.34 | 0.3 | mol $m^{-2}$ $s^{-1}$ |
| Characteristic leaf length | $l_c$ | 0.1 | – | 0.1 | 0.1 | m |
| Emissivity, long-wave, leaf | $\epsilon_{IR}$ | 0.96 | 0.96 | 0.96 | 0.96 | – |
| Boundary layer conductance (one side, cuvette) | $g_{bl}$ | 1.42 | 1.42 | – | – | mol $m^{-2}$ $s^{-1}$ |
| Wind speed | $u_w$ | 3.86 | – | 3.86 | 3.86 | m $s^{-1}$ |
| Relative humidity | RH | 44% | 84% | 85% | 44% | – |
| Temperature, air (base) | $T_{air}$ | 301.5 | 298.15 | 301.5 | 301.5 | K |
| Photosynthetic photon flux density | PPFD | 1,700 | – | 1,700 | 50–2,000 | $\mu$mol $m^{-2}$ $s^{-1}$ |

[a]Dashes indicate a dimensionless (unitless) quantity.

Based on a simple 1D volume-weighted average water potential (Eq. 22), the predicted average water potential for these leaves $\langle\psi\rangle$ was −1.81 MPa, while the value predicted by an equation accounting for the effect of the three-dimensional (3D) geometry of the vein-tissue interface on water potential gradients (Eq. 23) was −1.72 MPa. This latter value was within the measurement error (±0.034 MPa; Rockwell, 2010) of the actual average water potential $\psi_{leaf}$ measured with the pressure chamber, −1.73 MPa ($n$ = 5, ±0.14 SD); we regard this agreement as partial validation of the model. As a point of reference, the apparent $K_{leaf}$, or transpiration divided by the difference between covered ($\psi_r$) and transpiring leaf water potentials [$K_{leaf} = E/(\psi_r - \psi_{leaf})$], was 13.3 mmol $m^{-2}$ $MPa^{-1}$ $s^{-1}$, within the range of values reported by Sack et al. (2002).

*Solution for an Exposed-Leaf Energy Balance*. The solution of the model for an exposed leaf (i.e. with an environmental rather than within-cuvette energy balance) yielded nearly identical results for the distribution of evaporation (Fig. 2). With the average leaf water potential as a constraint, the solution implies values of absorptance ($a_{SR}$ = 0.4) and reflectance ($r$ = 0.15) at the low end of the expected range (Nobel, 2005) but reasonable considering that leaf angles were assumed to be ideal.

With no vapor flux leaving the upper epidermis, we find that the palisade remains close to the water potential of the transpiration stream where it exits the veins, whereas there is a large water potential drop from the vascular plane to the stomata in the lower epidermis (Fig. 2A). The spongy mesophyll, therefore, represents the dominant hydraulic resistance to $E$. As the palisade has a larger volume and is denser in cells than the spongy mesophyll, we further found that the average water potential of the whole leaf remains close to the water potential at the vascular plane, −1.68 MPa. As a result, $K_{leaf}$ reports the effective vascular conductance from the petiole to the vascular plane, $\varsigma h_A$, rather than the extravascular tissue hydraulic resistance dominant in transpiration. This scaling of $K_{leaf}$ with vascular, rather than mesophyll, hydraulic conductance is likely to be the general case for hypostomatous leaves.

Leaf temperature peaked in the palisade (Fig. 2B), with a small drop toward the upper nontranspiring epidermis. In accordance with this temperature drop toward the upper surface, the model predicts a small flux of vapor that condenses at the nontranspiring epidermal surface (Fig. 2, C and D) and flows back toward the palisade as liquid (Fig. 2, A and D). This circular flow above the temperature peak is interesting, as it acts as a heat pump (Chen et al., 2014), moving energy absorbed in the palisade to the upper (adaxial) epidermis, although here the effect is small: a molecular flux less than 1% of transpiration carrying less than 1% of the energy load in the upper domain. With larger air fractions in the palisade, this effect will become more important.

In both domains, we found a strong tendency toward heat conduction over local evaporation and latent transport, as indicated by values of $\Pi_\psi$ much larger than 1 (8.9 and 55.2 in the lower and upper domains, respectively). The larger value of $\Pi_\psi$ in the palisade is driven by the lower air fraction (0.05) versus the spongy

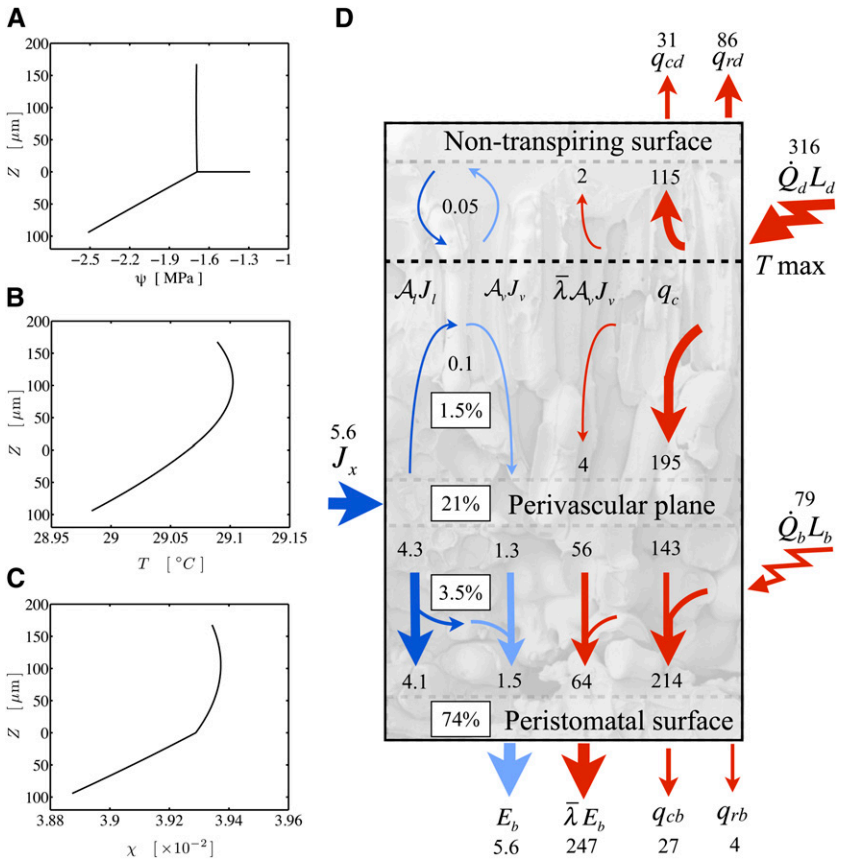


**Figure 2.** Solution of the model for an oak leaf with gas-exchange, hydraulic, and anatomical data. A, Water potential profile with the vascular plane at $z = 0$. The horizontal line is the potential drop between the stem and the vascular plane. B, Temperature profile. C, Mole fraction profile. D, Fluxes of energy (red; W $m^{-2}$) and molecules (dark blue for liquid and light blue for vapor; mmol $m^{-2}$ $s^{-1}$) and the percentage of the total transpirational phase change occurring in different regions of a leaf. Conduction ($q_c$; total of both phases) is the dominant mode of absorbed energy dissipation internally within both domains. In the upper domain, a small flux of vapor to the upper epidermis condenses and flows back into the palisade to reevaporate, with a net flux of latent heat to the upper surface.

domain (0.3) and is why only 1.5% of $E$ originates in the palisade, where 80% of the energy load is absorbed. Rather, thermal conduction to the upper epidermis accounted for about one-third of the short-wave load absorbed in the palisade (36%), with the largest fraction being conducted to the vascular plane (62%). At the vascular plane, a large fraction (17%) of the load absorbed in the upper domain drives evaporation (21% of $E$), yet almost half (45%) of the upper domain load is ultimately conducted to the lower epidermis, where it contributes to a dominant peristomatal fraction of evaporation (74% of $E$; Fig. 2D).

Thus, in this system, evaporation occurs in the first region in which the transpiration stream encounters a vapor phase (perivascular) and from the wet surfaces proximal to the stomata and the undersaturated external air (peristomatal). Two factors appear to be important for perivascular evaporation. First, as the air fraction is larger in the spongy than the palisade mesophyll, thermal conduction away from the vascular plane is less efficient than that to it (Fig. 2D), and the larger spongy air fraction also makes latent transport in the vapor phase more competitive. Second, the direction of the water potential gradient (Fig. 2A) promotes vapor diffusion below the vascular plane (Eq. 7) but impedes it above. As these two factors are quite general for hypostomatous leaves, perivascular evaporation may be a widespread phenomenon and the contribution to $E$ of evaporation from the walls of photosynthetic mesophyll cells a minor component.

The above distribution of evaporation within red oak, although varying to a small extent with transpiration and the energy fluxes, is expected to be resilient, based on both perturbations to the full model (Supplemental Fig. S1) and an analysis of Equation 14 for the peristomatal fraction. The leaf structural component of the peristomatal fraction (Eq. 14) dominates the environmentally sensitive term (Eq. 15), 0.753 versus −0.014; the small value of the latter term reflects the fact that the latent flux is much greater than the sum of the conductive and long-wave fluxes from the lower epidermis (Fig. 2D). We expect that for similar mesic hypostomatous leaves, the pattern of dominant peristomatal evaporation, with most of the balance perivascular, should be robust over a wide range of conditions.

### *The Control of Transpiration by Radiation as Modeled for a Sunflower Leaf*

We next sought to investigate the control of transpiration by radiation and to model internal transport in an amphistomatous leaf (both domains transpiring) based on experimental data for a sunflower leaf (Pieruschka et al., 2010) and sunflower leaf structure (Dengler, 1980). In the cited sunflower leaf experiment, the near infrared (NIR) load on the leaf was manipulated by the use of a

cold mirror, such that absorbed short-wave radiation could be increased from 160 to 200 W $m^{-2}$ with no change in photosynthetic photon flux density (PPFD; Fig. 1 in Pieruschka et al., 2010). Following the increase in NIR, $g_s$ and transpiration were both observed to increase by approximately 10%, a phenomenon described by those authors as control of transpiration by radiation, and we were interested to see whether our mixed transport model could produce a similar result. As we could not constrain all the model parameters with the available data, some parameters had to be assumed; leaf thicknesses, tissue thermal and hydraulic conductivities, area fractions, the distribution of absorbed energy between the two domains, and leaf vascular conductance were chosen within a plausible range that reproduced the transpiration rate, $g_s$, and leaf-to-air mole fraction gradient reported by Pieruschka et al. (2010).

We first assumed a simple linear relation between steady-state $g_s$ and epidermal water potential for small perturbations around an observed value (hydraulic model) based on the form of turgor and aperture curves described by Franks and Farquhar (2007); this step was taken to relax the assumption in the model of Pieruschka et al. (2010) that stomata adjust to conserve a fixed target water potential. With the parameters in Table III, the amphistomatal model for the initial state of absorbed shortwave radiation ($SR$) = 160 W $m^{-2}$ predicts a slight dominance of internal vapor transport (56% of total $E$) over total peristomatal evaporation (44%), with the dominant fraction (42%) occurring as perivascular evaporation and diffusion toward the lower epidermis (Fig. 3D). As for oak, we find evaporation in either mesophyll contributes only in a minor way to the evolution of $E$ (14% in aggregate). Interestingly, the evaporative flux in the palisade is almost equally split in its contributions to $E$ from the lower and upper surfaces (4% and 6% of total $E$, respectively), as the water potential gradient toward the upper epidermis is not strong enough to drive vapor across the temperature maximum (Fig. 3D).

Following an increase in NIR such that $SR$ = 200 W $m^{-2}$ and an adjustment to air temperature to hold the lower epidermis at nearly constant temperature (Pieruschka et al., 2010), the hydraulic model (i.e. including a hydraulic stomatal response) predicted about half the observed response in total $g_s$ (6% versus approximately 10%), with all of the increase occurring for the lower epidermis (Fig. 3E). This increase in $g_s$ was driven by an increase in lower epidermal water potential (from −0.9 to −0.82 MPa), which in turn occurred due to a decrease in the liquid flux (and the proportion of peristomatal evaporation) even as transpiration increased (by 4.4%). Liquid transport decreased in absolute terms because the increase in the internal temperature gradients that accompanied the higher energy load drove an increase in vapor transport sufficient to displace part of the initial liquid flux; in terms of the percentage of $E$, total peristomatal evaporation decreased (from 44% to 38% of $E$) while internal vapor transport increased (from 56% to 62% of $E$).

We did, however, find that with a hydraulic feedback model for stomatal aperture, the positive effect of the higher energy load on stomatal aperture was dependent on the 0.4°C reduction in air temperature required to conserve lower epidermal temperature, which otherwise saw a small increase in lower $g_s$ offset by a decrease in upper $g_s$. However, Pieruschka et al. (2010) state that the observed response was not entirely dependent on such temperature adjustment. A second series of analyses of the cold-mirror experiment, following Pieruschka et al. (2010) in assuming that stomata adjust to conserve a fixed target epidermal water potential, confirmed that this was possible in our model as well (Supplemental Fig. S2, A and B).

To understand what influences the magnitude of the stomatal response in a conserved epidermal water potential model, we start with the proposition that an increase in transpiration can occur in one of two ways: an increase in $g_s$ or an increase in epidermal temperature and, therefore, the leaf-to-air vapor mole fraction difference, $\Delta\chi$. At the same time, dissipating an increased energy load requires an increase in the internal temperature gradient from the sites of short-wave absorption to the leaf surface, such that both the flux of internal vapor and thermal conduction increase. To have an increase in internal vapor transport that is passed through to $E$ via an increase in $g_s$, therefore, requires that the extra energy conducted to the epidermis be transmitted to the environment as efficiently as possible, minimizing the increase in surface temperature and $\Delta\chi$ that would compete with $g_s$ to explain an observed increase in $E$.

Formally, considering a single domain subject to a radiative load $SR$, holding the epidermal water potential and, therefore, the liquid flux constant leads to an expression for the change in total conductance, $\delta g_T$ (inclusive of stomatal and boundary layer effects), that results from an additional radiative load $\delta SR$ (Supplemental Text S2) as:

$$\frac{\delta g_T}{g_T} = \frac{\delta SR}{\bar{\lambda}E}\left[1 - \frac{\mathcal{A}_l k_l^T + \mathcal{A}_v k_v^T}{\mathcal{A}_l k_l^T + \mathcal{A}_v k_v^T + \mathcal{A}_v \bar{\lambda} c D_v \chi_T}\left(1 + \frac{\bar{\lambda} g_T \chi_T}{k_s^T}\right)\right]$$

$$k_s^T = \frac{q_r + q_s}{\Delta T_{ea}} \tag{20}$$

The ratio of the increase in thermal load ($\delta SR$) to the initial latent flux ($\bar{\lambda}E$) sets the maximum positive response. The second ratio ranges from 1:1 to a plausible limit of 1:3 as internal latent transport due to thermal gradients becomes important relative to internal thermal conduction; the third and final ratio describes the sensitivity of latent transport from the leaf to temperature, $\bar{\lambda} g_T \chi_T$, relative to sensible conductivity $k_s^T$ (inclusive of net long-wave radiation and conduction). This last ratio says that stomatal opening in response to increased energy load is aided by low initial $g_s$ values and confirms the importance of efficient conductive

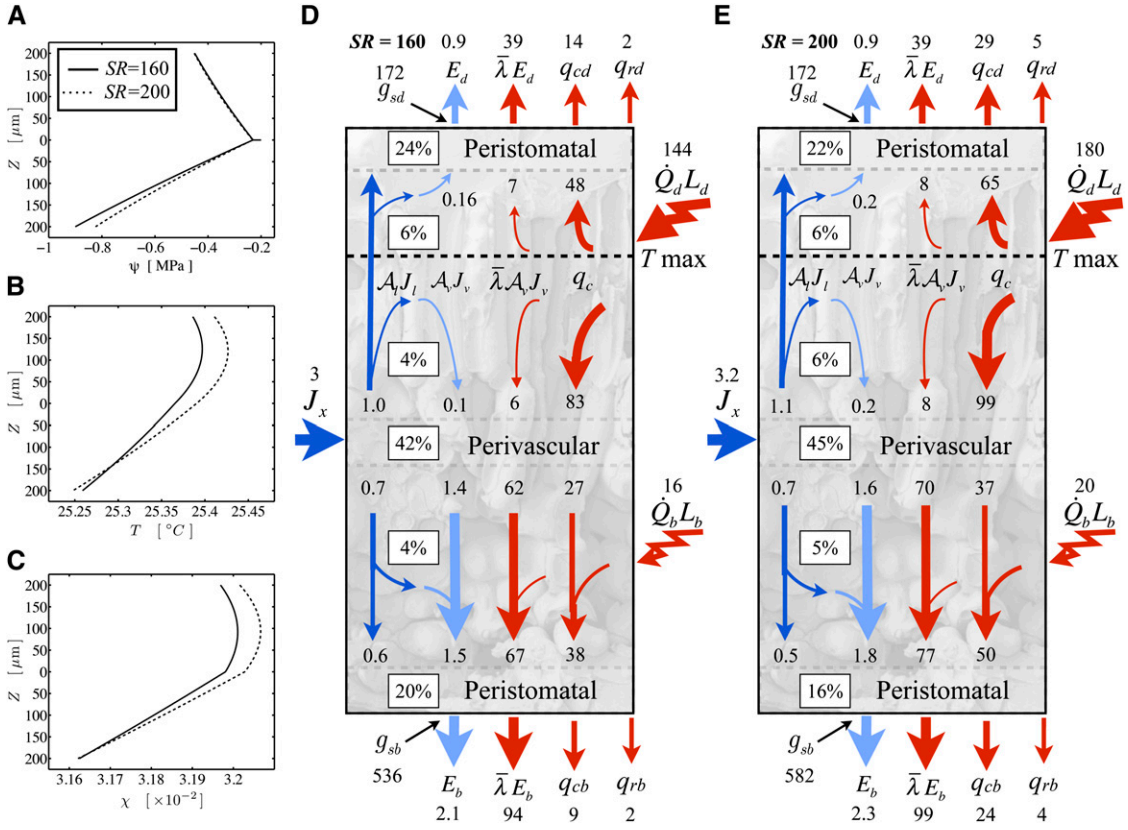


**Figure 3.** Model results for a sunflower leaf illuminated by a cold mirror (*SR* = 160 W m$^{-2}$; solid lines) and a full mirror (*SR* = 200 W m$^{-2}$; dashed lines), as in the experiments of Pieruschka et al. (2010). A, Water potential profile through the leaf thickness (upper = adaxial, lower = abaxial) with the vascular plane at $z = 0$. The horizontal line is the potential drop between the stem and the vascular plane. B, Temperature profile. C, Mole fraction profile. D and E, Fluxes of energy (red; W m$^{-2}$) and molecules (dark blue for liquid and light blue for vapor; mmol m$^{-2}$ s$^{-1}$) and the percentage of the total transpirational phase change occurring in different regions of a leaf, under illumination by a cold mirror (*SR* = 160; D) or a full mirror (*SR* = 200; E). Under the higher thermal load, an increase in internal temperature gradients shifts more of the water flux from liquid to vapor.

and radiative energy transfer to the environment that minimize increases in leaf surface temperatures.

Interestingly, while both condensation (Eq. 17) and a positive stomatal response (Eq. 20) are favored by a dominance of latent transport due to thermal gradients over heat conduction inside the leaf and a dominance of sensible heat over latent heat at the surface, their expressions are not identical. Leaves that achieve a condensing state on the inner face of a transpiring epidermis are likely also to be in a regime where stomatal aperture increases for a higher short-wave load, but the converse is not true. The more restrictive condition for condensation requires that the sensible flux from the surface be at least more than half as large as the latent flux, given that, even for the extreme case of a 90% air fraction in the lower domain and a thermal conductivity for the cells one-third that of water, the ratio of thermally induced latent to sensible internal heat transport in Equation 17 is less than 2.

A final result of the model containing a hydraulic feedback on stomatal aperture underscores the point that average leaf water potentials (as measured by a pressure chamber or psychrometer) cannot be expected to follow a simple relationship with the water potential of a transpiring epidermis. For example, in the hydraulic feedback analyses (Fig. 3), lower epidermal water potential increased by 0.08 MPa with the increase in energy load, even as the average water potential of the leaf increased by only 0.015 MPa. In addition, these problems extend to measures of hydraulic transport efficiency that depend on average leaf water potential, such as $K_{leaf}$, which increased in the hydraulic feedback model by 12.5% (8.2–9.2 mmol m$^{-2}$ MPa$^{-1}$ s$^{-1}$) between the cold- and full-mirror treatments, despite constant parameter values for the hydraulic conductivity of the xylem or cells.

### *Condensation and Energy Overload in an Oak-Like Leaf*

We next sought to understand the implications for transport efficiency and stomatal control of a hypostomatous leaf pushed by increasing energy loading into a condensing state at its transpiring epidermis. We started with a leaf characterized by parameter values for red oak and increased the air fraction to 85% in the spongy

and 20% in the palisade (43.4% overall) to produce a leaf with $\Pi_{\psi}$ of 12.6 in the palisade and 3.5 in the spongy (Table III). For this leaf, internal vapor transport accounted for 103.8% of $E$ (condensing flux = 3.8% of $E$) under conditions of 85% relative humidity and 1,700 $\mu$mol m$^{-2}$ s$^{-1}$ PPFD ($SR$ = 394.9 W m$^{-2}$). The high relative humidity was necessary to suppress $\lambda$E and so increase the magnitude of the first term in the peristomatal Equation 14 over the second ($-0.236$ versus 0.198); as a result, even for a large spongy air fraction, reaching a condensing state at the lower epidermis required a leaf surface temperature more than 2°C above ambient. We then compared the effects on internal transport of dropping or increasing the energy load by 100 W m$^{-2}$: the high- and low-load final states are shown in Figure 4 (initial state not shown).

Dropping the energy load by 100 W m$^{-2}$ pushed the leaf out of the condensing regime, with peristomatal evaporation at 2% (Fig. 4D); the leaf-to-air temperature difference fell to 1.5°C, but the change in epidermal water potential (+0.03 MPa) resulted in no material change in $g_s$ (Fig. 4D). Nor did the opposite perturbation, adding 100 W m$^{-2}$, result in an increase in $g_s$ as hypothesized by Pieruschka et al. (2010), despite the existence of a condensing flux equivalent to 8% of $E$ (Fig. 4E). The smaller total vascular-to-epidermal water potential difference in the lower domain was offset by the increased drop through the leaf vasculature and stem accompanying the increased flux. The difference from the sunflower simulations is not only the lack of compensatory changes in air temperature but that here we account for hydraulic feedbacks due to larger water potential drops through the root and stem arising from higher fluxes at the whole-plant level as well.

Considered from the perspective of stomatal protection of either the leaf tissue or xylem from excessively low water potentials, the model results suggest that condensing steady states may be maladaptive to the extent that stomata are influenced by epidermal water status. While the water potential at the transpiring surface dropped by 0.06 MPa between the low- and high-energy loads in Figure 4, the water potential at the vascular plane fell 0.24 MPa and the average water potential of the mesophyll by 0.21 MPa. This sort of uncoupling, increasing with higher energy loads and $E$, indicates that condensing states, although apparently hydraulically efficient in the sense that $K_{leaf}$ increased from 14.2 to 17.1 mmol m$^{-2}$ MPa$^{-1}$ s$^{-1}$ between $SR$ = 295 and 495, could lead to the loss of tight stomatal control of xylem tensions.

### *Modeling Evaporative Flux Experiments on Detached Leaves*

In the condensing leaf simulation (Fig. 4), the increase in apparent $K_{leaf}$ found for a 200 W m$^{-2}$ increase in energy load, equivalent to about an 800 $\mu$mol m$^{-2}$ s$^{-1}$ increase in PPFD, amounted to a 20% increase over the initial value, with only a 1.5°C change in epidermal temperature that, from the perspective of viscosity corrections, might be considered nonsignificant. As an experimental result, this might easily be mistaken as evidence of an increase in the permeability of the cells. Therefore, we sought to understand to what extent evaporative flux measures of $K_{leaf}$ are sensitive not just to leaf temperature but also to the balance of sensible and latent fluxes from the surface, which can change the length of the flow path by changing the peristomatal fraction, as in Equation 17.

At any particular epidermal surface temperature, average leaf water potential is sensitive to a shift in the balance of internal liquid versus vapor transport, such that leaves with more internal vapor transport have a higher apparent $K_{leaf}$. The problem for experiments on detached leaves is exacerbated by the fact that stomata may be difficult to open under conditions of high water potential due to the mechanical advantage of the epidermis (Brodribb and Holbrook, 2006; Franks and Farquhar, 2007). To make the point concrete, we modeled a detached leaf with the hydraulic and thermal properties of oak leaves, and a volumetric air fraction of 34% more representative of leaves broadly (Byott, 1976), in shade and full sun (50 and 2,000 $\mu$mol m$^{-2}$ s$^{-1}$ PPFD, respectively), with $g_s$ constrained to 50 and 100 mmol m$^{-2}$ s$^{-1}$, respectively (Fig. 5). $K_{leaf}$ increased 55% between the two radiation levels, even when air temperature was adjusted to conserve epidermal temperature. Therefore, we caution that the apparent $K_{leaf}$ can change depending on the details of the energy regime, despite negligible changes in surface temperatures, even as the hydraulic conductivity of the cells remains unchanged. This effect is expected to be particularly pronounced when a leaf shifts from a cool leaf regime (energy loading dominated by conduction to the epidermal surfaces, favoring peristomatal evaporation) to a warm leaf regime (energy loading dominated by short-wave absorption in the mesophyll), as shown here (Fig. 5, D and E).

## DISCUSSION

Our analysis of evaporation in leaf tissue found that a single nondimensional parameter group, $\Pi_{\psi}$, describes the competition of sensible and latent heat transport. This parameter group depends not only on the physical properties of air and water, as in the equilibrium evaporation case (Raupach, 2001), but also on the sensitivity of vapor pressure to liquid phase water potential within the mesophyll and the hydraulic and thermal conductivities of leaf tissue as well. Unless the chemical potentials of the vapor and liquid phases of water in mesophyll airspaces and cells are far out of local equilibrium, as for example due to an extensive internal cuticle in the mesophyll, our analysis should provide a reasonable guide to thinking about the coupling of heat and molecular transport in leaves. And, in any case, our analysis demonstrates the importance of accounting for liquid phase thermal conduction.

Indeed, liquid phase thermal conduction appears to be not only important but inevitable. Under local

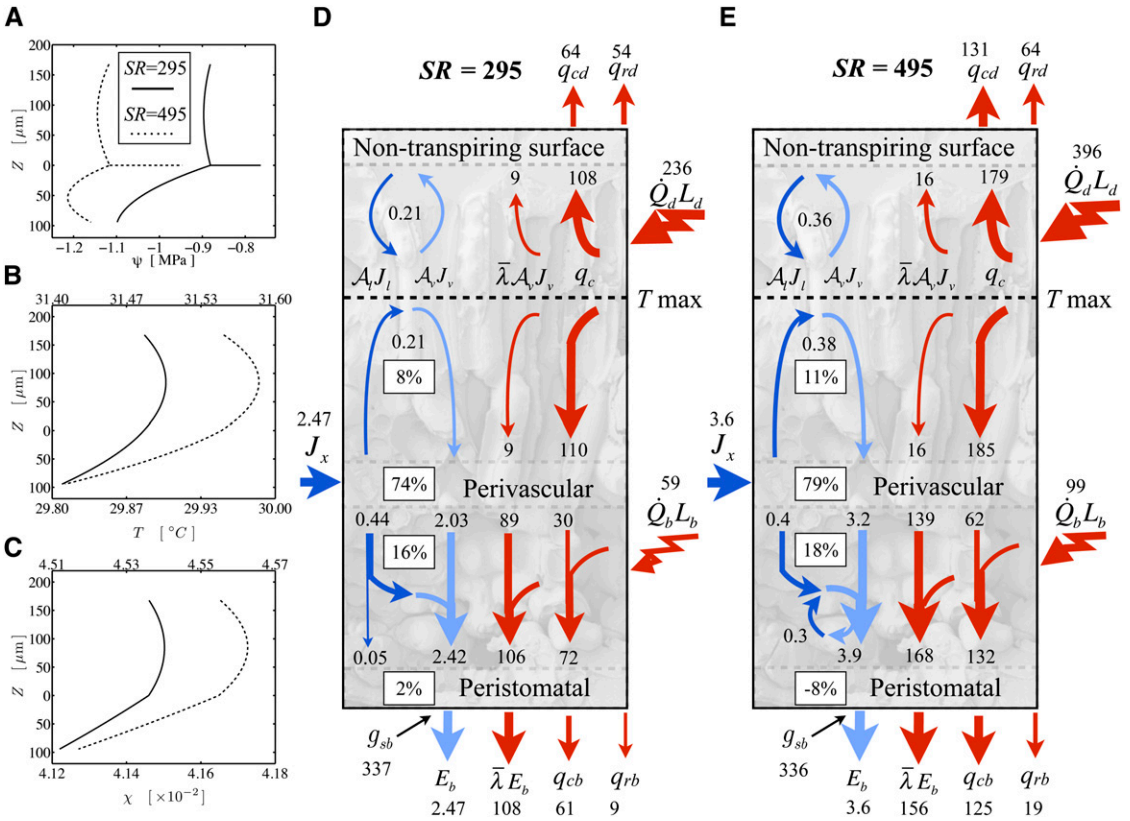


**Figure 4.** The shift at higher short-wave radiation loads to a condensing state at the lower epidermis in an oak-like leaf with an air fraction of 0.434. For A to C, solid lines are for the low load (*SR* = 295 W $m^{-2}$) and dotted lines are for the high load (*SR* = 495), with the scale on the top *x* axis in B and C. A, Water potential profile through the leaf thickness (upper = adaxial, lower = abaxial) with the vascular plane at $z = 0$. The horizontal line is the potential drop between the stem and the vascular plane. B, Temperature profile. C, Mole fraction profile. D and E, Fluxes of energy (red; W $m^{-2}$) and molecules (dark blue for liquid and light blue for vapor; mmol $m^{-2}$ $s^{-1}$) and the percentage of the total transpirational phase change occurring in different regions of a leaf under a low short-wave load (*SR* = 295; D) and a high load (*SR* = 495; E). The high load pushes the internal face of the lower epidermis into a condensing state (the internal evaporative flux exceeds transpiration), such that there is a small liquid flux back into the spongy mesophyll, where it reevaporates.

equilibrium, both vapor and liquid tend to move down gradients in water potential; however, the vapor flux has an additional tendency to move down temperature gradients, as can be seen in Equation 7. For water to evaporate locally, the water potential gradient out of the local volume must be less steep than the gradient in, such that more liquid water moves in than out. But this also means that the component of the vapor flux due to water potential is greater in than out, the opposite of what is required to have a net increase in vapor out of the local volume. Molecular conservation then requires that the component of vapor diffusion due to the temperature gradient be greater out than in, such that the resulting vapor mole fraction gradient is greater out than in. This constraint of molecular conservation on the temperature gradient means that thermal conduction will also be greater out than in, such that the absorbed energy load can never be dissipated solely by latent transport; some energy will also flow out by thermal conduction.

Our subsequent analyses of particular cases are not intended as definitive descriptions of the distribution of evaporation in transpiring leaves; rather, they are put forward as a first-order framework for organizing thinking about both the competition between liquid and vapor transport and the competition between latent heat and thermal conduction. For example, the 1D model structure is clearly violated by the discrete placement of veins and stomata in leaves. While the issues of vein spacing can be addressed by way of a correction factor, based on simulation of the full 3D geometry of an areole (Rockwell et al., 2014b), as done here for oak, understanding the effects of discrete stomatal spacing and the geometry of substomatal cavities (Pickard 1982), as well as internal cuticle (Pesacreta and Hasenstein, 1999), on the water potential and temperature of the peristomatal region requires further work. Finer scale physical detail, such as volume fractions for specific tissues, rather than averaged over whole domains, as well as independent estimates of a

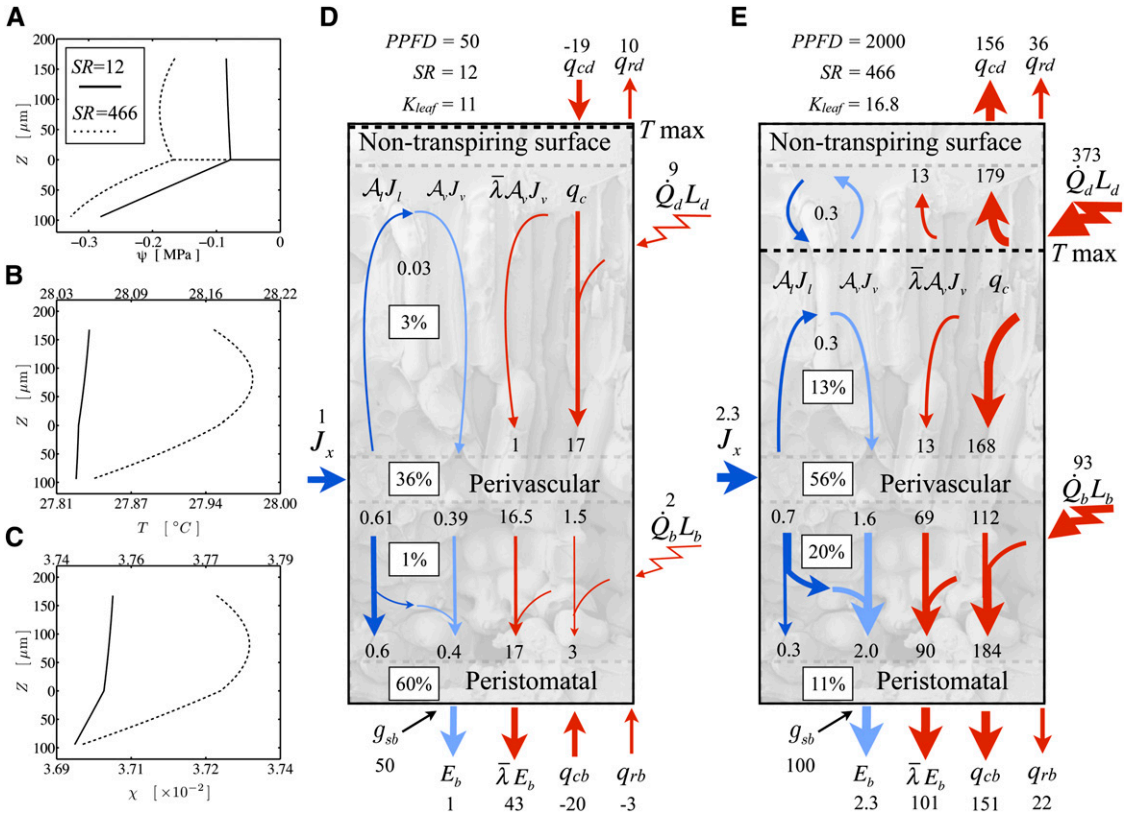


**Figure 5.** Distribution of evaporation for a simulated low-light (PPFD = 50 $\mu$mol m$^{-2}$ s$^{-1}$) evaporative flux experiment on an oak-like leaf but with an air fraction of 0.34. For A to C, solid lines are for the low load ($SR$ = 12 W m$^{-2}$) and dotted lines are for the high load ($SR$ = 466), with the scale on the top $x$ axis in B and C. A, Water potential profile through the leaf thickness (upper = adaxial, lower = abaxial) with the vascular plane at $z$ = 0. The horizontal line is the potential drop between the stem and the vascular plane. B, Temperature profile. C, Mole fraction profile. D and E, Fluxes of energy (red; W m$^{-2}$) and molecules (dark blue for liquid and light blue for vapor; mmol m$^{-2}$ s$^{-1}$) and the percentage of the total transpirational phase change occurring in different regions of a leaf under two different energy regimes, driven by low (D) and high (E) light levels ($\mu$mol m$^{-2}$ s$^{-1}$). The transition from a dominant surface load of sensible heat at low light to a dominant short-wave load at high light results in a large change in $K_{leaf}$ (mmol m$^{-2}$ MPa$^{-1}$ s$^{-1}$).

tortuosity for the vapor path, could further fine-tune these analyses. More detailed short-wave absorption functions could also be incorporated (Knipling, 1970), yet given the apparent strength of thermal conduction in leaf tissue, the exact pattern of absorption within a domain seems unlikely to have a strong effect on the results. The assertion of a well-defined steady state for transpiring leaves might also be questioned. Philip (1966) estimated, based on the characteristic times for the propagation of water potential changes in plant tissue versus the typical period of environmental variation, that as long as $g_s$ is stable, leaves attain physically well-defined steady states, although a transient analysis may be necessary to understand behavior at the wilting point. Here, if we accept the apparent stability of gas-exchange measurements, the argument of Philip (1966) supports steady water potential and temperature profiles through the leaf tissue as well.

With all of the above caveats, a number of general points pertaining to leaf structure and function emerge from our analysis. The distribution of evaporation found here for oak provides a general model for hypostomatous leaves with smaller airspaces in the palisade than spongy mesophyll: due to the high thermal conductivity of leaf tissue and small airspaces, heat conduction is more efficient than latent heat transport for dissipating the large absorbed radiation load in the palisade. At the transition to the spongy mesophyll (i.e. the perivascular plane), the increase in air fraction increases the competitiveness of vapor transport, so some of the conducted heat flux switches to latent transport, creating perivascular evaporation. Local evaporation in the spongy mesophyll is low, as the local radiation load is small. The remainder of the heat conduction flux that originated in the palisade (and was not consumed by perivascular evaporation) ultimately arrives at the lower epidermis, where it provides the energy for peristomatal evaporation and for the surface sensible fluxes. For such leaves, mesophyll evaporation will be a subordinate component, with the dominance of either perivascular or peristomatal evaporation strongly

influenced by the amount of airspace in the spongy mesophyll.

More broadly, given that the hydraulic conductivity of the cells may span 1 order of magnitude larger and smaller than found here for oak (Kramer and Boyer, 1995), that volumetric air fractions span 2% to 55% of total leaf volume and may reach 70% in the spongy mesophyll of some leaves (Pieruschka et al., 2010), and that the thermal conductivity of the cells is not likely to be much less than that of water (Tyree and Yianoulis, 1980), we should expect that leaves span nearly the full range of peristomatal fractions. The crucial role of the extent of spongy mesophyll airspace in shifting evaporation between peristomatal and perivascular regions may then reconcile evidence for a dominant role of vapor transport in plants that have extensive airspaces (Boyer, 1985; Mott, 2007) versus evidence for the dominance of peristomatal evaporation in plants with denser spongy mesophyll (Byott and Sheriff, 1976). Indeed, given the importance we find for heat conduction in the liquid phase, most of the variation in the distribution of evaporation between leaves may occur as differences in perivascular evaporation (evaporation into the first available airspaces) versus peristomatal evaporation (evaporation from the wetted surfaces closest to the unsaturated external air). Nevertheless, mesophyll evaporation will be somewhat higher in leaves with a lower peristomatal fraction, as low values of $\Pi_\psi$ favor both local evaporation and vapor transport from the vascular plane.

The distribution of evaporation within a given leaf, however, is not static. As the tendency toward vapor transport increases ($\Pi_\psi$ approaches 1, and the bracketed term in the peristomatal Eq. 14 goes to 0), the internal distribution of evaporation becomes more sensitive to the surface fluxes and environmental conditions. An increase in transpiration due to a decrease in ambient mole fraction pulls the distribution of evaporation toward the stomata. On the other hand, an increase in transpiration due to an increase in the energy load absorbed in the mesophyll reduces the peristomatal fraction, as the resulting increase in the temperature gradient shifts the balance of molecular transport toward the vapor phase. As the latter effect is more likely to be important in driving $E$ on diurnal time scales, the resulting shifts in evaporation sites may help explain the inverse relationship in oxygen isotope studies of leaf water between transpiration and the effective pathlength from the veins to the sites of evaporation (Song et al., 2013).

Another important point that emerges from the analysis is that experiments to characterize hydraulic transport properties of transpiring leaves need to account for the energy-loading regime and not simply leaf surface temperatures. Even for the transpiring oak leaves modeled here, with a strong dominance of the liquid path at 74% peristomatal evaporation, temperature-induced vapor movement explained 11% of the internal flux, such that accurate characterization of leaf-averaged hydraulic parameters based on transpiration (nonisothermal) experiments requires accounting for internal temperature gradients. Comparisons of $K_{leaf}$ between heavily shaded leaves, below ambient air temperature when the external latent heat flux exceeds the solar short-wave load, and an identical illuminated leaf for which the opposite is true may be expected to be problematic. This will be especially true for leaves with large air fractions, as these can shift from a dominantly peristomatal to a dominantly perivascular evaporative regime between cool and warm states.

A final point, pertaining to stomatal behavior, is that our model concurs with the core hypothesis of Pieruschka et al. (2010) that, under some circumstances, increases in short-wave radiative loading that drive a larger internal vapor flux could lead to increased stomatal apertures. However, we find that it is not necessary for the internal surface of the leaf to be in a condensing state for this effect to occur. To the extent that stomatal regulation emphasizes water over energy balance, such condensing states may indeed be pathological.

The specific cases examined here are just the first steps in elucidating the adaptive significance of internal vapor versus liquid transport. While the theoretical analyses presented here provide a broad outline, reconstructing the distribution of evaporation (i.e. as done here for red oak) for a variety of leaves with varying internal architectures, characteristic environments, and growth habits will be required to fill in the picture. With respect to water use efficiency, there would not appear to be any obvious first-order effects of internal vapor versus liquid transport. The most important factor for transport influences on water use efficiency are leaf-to-air temperature differences (a cooler leaf will be more water use efficient), and these do not seem particularly sensitive to which mode of internal transport is dominant.

In contrast, the hydraulic efficiency of the leaf, defined as $E$ divided by the vascular-to-epidermal water potential drop, will be very sensitive to the amount of vapor phase transport. The more the internal $E$ is driven by temperature-induced gradients in the mole fraction, the shallower the water potential gradient from veins to transpiring epidermis will be. As seen in the sunflower simulations, such temperature effects mean that increases in energy loading are accompanied by increases in hydraulic efficiency, such that the water potential gradient may change little as $E$ fluctuates with a varying solar load. A large perivascular fraction of $E$ could then save the construction costs associated with building stiff tissues capable of maintaining volume homeostasis over large swings in water potential.

What, then, might be the risks of, or constraints on, using temperature-induced vapor transport to move water to the stomata? The temperature sensitivity of vapor phase transport may help mitigate solar load-driven demand shocks but will not help with supply shocks due to soil drying. Where leaves must function over a wide range of soil water potentials during their lifetime, it may be more advantageous to invest in stiff epidermal tissues capable of sustaining the water potentials

necessary to extract water from drying soils. In addition, the condensing leaf simulation (Fig. 5) points to a possible constraint in that if a leaf with a high perivascular fraction is pushed into a state where condensation occurs at the transpiring epidermis, protection of the vasculature from excessive tensions could be compromised.

A final hypothesis suggested by the energy component of this analysis relates to the functional significance of bundle sheath extensions. A role for these structures in providing a low-resistance path for flow to a transpiring epidermis has long been suggested (Wylie, 1952). The fact that they have been found to be more prevalent in upper canopy (high-energy) rather than subcanopy (low-energy) strata (Kenzo et al., 2007) suggests a role in aiding thermal conduction of energy absorbed in the upper epidermis and palisade to what we find to be the dominant sites of evaporation, the perivascular and peristomatal regions.

The theoretical and experimental analyses presented here demonstrate that consideration of the competition between liquid and vapor, as well as thermal conduction and latent heat, provides an essential perspective for understanding leaf structure and function. The descriptions of leaf structure that enter into the 1D analysis are still very rudimentary, however. Fortunately, the modeling approach taken here is sufficiently general that more detailed descriptions of leaf architecture (e.g. the locations of internal cuticles, veins, and stomata) can be realized in the future by relaxing local equilibrium and implementing the model in a numerical simulation package. Even so, the analytical results presented here for the distribution of evaporation, and the parameter $\Pi_\psi$, will likely retain their value for developing an intuitive understanding of where the transpiration stream changes phase inside leaves.

## MATERIALS AND METHODS

### Parameterization and Solution of the Transpiring Oak Leaf Model

#### *Solution for a Section of Leaf Enclosed in a Cuvette*

For leaves of northern red oak (*Quercus rubra*), we estimated $h_A$, $k_l$, $A_l$, and $A_v$ based on hydraulic and anatomical experiments. To estimate the liquid phase hydraulic conductivity for red oak, we used data from rehydration experiments conducted on bagged leaves initially attached to a tree on the campus of Harvard University (Rockwell et al., 2011). The results of these rehydration experiments, conducted on bagged leaves initially attached to the tree, were reported in terms of the ratio of final to initial water potential ($\Psi = \psi_f/\psi_o$) and the hydration time $t$. From these data, estimates of the total hydraulic conductivity of leaf tissue $k_t$ were calculated according to:

$$k_\ell = \xi \frac{4}{\pi^2} \ln\left(\frac{8}{\Psi\pi^2}\right) \frac{c_\ell^{1D} L^2}{t + \eta \ln(\Psi) \frac{2c_l L}{h_A}} \tag{21}$$

where $c_t$ is the volumetric hydraulic capacity of the leaf, $L$ is the half-thickness (i.e. the average length of the upper and lower domains), $h_A$ is the hydraulic conductance of the vascular network normalized to the leaf area, and $\xi$ and $\eta$ are scaling factors that map the 1D solution form to a numerical solution of the transient hydration in a 3D domain that respects the discrete placement of the vasculature (Rockwell et al., 2014b).

Flux measurements of transpiring leaves with a LI-6400 (Li-Cor Biosciences) provided the estimates of $E$, abaxial epidermal temperature ($T_{Lb}$), environmental air temperature ($T_{air}$), and boundary layer thickness ($\delta$). We then found the sensible heat flux $q_{cb}$ (Supplemental Text S1, Equation 1.28). In addition, taking the LI-6400 output TBlk as $T_{sur}$ with $a_{IR} = 0.95$ allowed estimation of the radiative flux $q_{rb}$ (Supplemental Text S1, Equation 1.25). The thermal conductivity of the liquid phase was estimated from a lateral thermal conductivity of oak leaves of 0.25 J m$^{-2}$ s$^{-1}$ K$^{-1}$ as reported previously (Vogel, 1983), yielding 0.286 J m$^{-2}$ s$^{-1}$ K$^{-1}$ after accounting for the air fraction. Volumetric air fraction was estimated from the weight gain observed for leaves submerged in water in a column subject to alternating cycles of pressurization at 0.1 MPa and vacuum until no further weight gain occurred (Byott, 1976). For comparison with the measured value $\psi_{leaf}$, the average water potential of the cells of a leaf (negligible density in the airspace), once at internal equilibrium, is given by:

$$\langle\psi\rangle = \frac{\mathcal{A}_{ld}\int_0^{Ld}\psi_d(z)dz + \mathcal{A}_{lb}\int_0^{Lb}\psi_b(z)dz}{\mathcal{A}_{ld}L_d + \mathcal{A}_{lb}L_b} \tag{22}$$

An estimate that takes into account the effects of vein spacing on water potential gradients is given by:

$$\langle\psi\rangle = \langle\Psi\rangle(\psi_r - \psi_e) + \psi_e,\ \langle\Psi\rangle = \phi + \frac{\omega}{\mathscr{B}} \tag{23}$$

where $\phi$ and $\omega$ can be predicted based on a leaf's internal geometry and $\mathscr{B}$ is the ratio of the vascular and tissue path conductances (Rockwell et al., 2014b).

In the initial iteration of the model (Supplemental Text S3), $q_{rd}$ and $q_{cd}$ were estimated assuming $T_{Ld} = T_{Lb}$, with the total absorbed short-wave load $SR$ then given by (Supplemental Text S1, Equation 1.35). The initial estimate of $\dot{Q}_b$ followed from (Supplemental Text S1, Equation 1.33). The physical properties $\overline{\lambda}, \chi_\psi, \chi_T, cD_v$ were then calculated at $T_{air}$ and $\psi_r$. To find $\psi_o$ for a hypostomatous leaf for which the vascular geometry is known, global molecular conservation (Supplemental Text S1, Equation 1.36) can be written in the form:

$$E = \mathfrak{s} h_A(\psi_r - \psi_o) \tag{24}$$

where $\mathfrak{s}$ is a correction factor that maps a 1D solution with a continuous vascular plane approximation to the numerical simulation of the full 3D problem with discrete vein placement, based on an analysis of the isothermal (linear) flow problem (Rockwell et al., 2014b). Essentially, $\mathfrak{s}$ accounts for the resistance to the lateral $(x,y)$ movement of water molecules in the vicinity of the vascular bundles, a resistance neglected in making a continuous vascular plane approximation that spreads vascular conductance smoothly over the whole vascular plane. For a hypostomatous leaf, the factor $\mathfrak{s}$ can be predicted from the vascular and tissue geometry that determines $\zeta$ and $\eta$ as well as the Biot number $\mathscr{B}$, the ratio of hydraulic conductance to the total conductance of the tissue between a vascular plane and the transpiring surface:

$$\mathfrak{s} = (\zeta\mathscr{B} + \epsilon)^{-1},\ \mathscr{B} = \frac{h_A L_b}{k_\ell} \tag{25}$$

For the first iteration, to find an appropriate value of $\mathfrak{s}$, we used the total effective hydraulic conductance of the tissue (the composite of air and cells) from the isothermal problem:

$$k_\ell = \mathcal{A}_l k_l + \mathcal{A}_v c D_v \chi_\psi \tag{26}$$

With this, the solution for the lower water potential field (Supplemental Text S1, Equation 1.23) was complete. Evaluating the solution for the lower temperature field (Supplemental Text S1, Equation 1.24) at $z = L$ with $T_{Lb}$ given by the temperature measured by the LI-6400 leaf thermocouple ($T_{leaf}$) provided an equation for $T_o$. Everything was then known.

For the second iteration, physical properties were recalculated at the first solution's values of $T_o$ and $\psi_o$. The upper surface heat fluxes $q_{rd}$ and $q_{cd}$ were recalculated for $T_{Ld}$, and the estimate of $SR$ was adjusted. In addition, the value of $\mathfrak{s}$ was updated from the first iteration of the solution by adjusting the effective hydraulic conductance of the tissue to account for the portion of the flux driven by temperature gradients:

$$k_\ell = \mathcal{A}_l k_l + \mathcal{A}_v c D_v \chi_\psi + \mathcal{A}_v c D_v \chi_T \left(\frac{T_o - T_{Lb}}{\psi_o - \psi_{Lb}}\right) \tag{27}$$

This process may be repeated for a third iteration to verify the stability of the solution, but this was not necessary for the red oak leaves studied here. Final parameter values are given in Table III.

#### *Solution for an Exposed Leaf*

We took $g_s$ as given (as measured in the cuvette), with $g_{bl}$ estimated from Supplemental Text S1, Equations 1.31 and 1.29 and with $l_c$ taken as 10 cm and $u_w = 1$ m s$^{-1}$. The mole fraction of the external air ($\chi_{air}$) was calculated

from the air temperature and humidity of the reference stream (bypass fully open) reported by the LI-6400. The transpiration rate was not imposed but depended on $\chi(T_{Lb}, \psi_{Lb})$ as given (Supplemental Text S1, Equation 1.30). The total solar load $SR$ was estimated from the energy per mole of incident photosynthetically active radiation (PAR), for the solar spectrum $2.35 \times 10^5$ W $mol^{-1}$, based on the observation that PAR contains about half the energy in the solar spectrum and that about half of incident solar short-wave radiation (PAR and NIR) is absorbed by leaves (Campbell and Norman, 1998). The source terms $\dot{Q}_b, \dot{Q}_d$ were then set by assuming a distribution of the solar load between spongy and palisade tissues, as in Supplemental Text S1, Equations 1.32 and 1.33. To calculate the net long-wave radiative fluxes on the upper and lower leaf surfaces, we let $T_{sur} = T_{sky}$ on the upper epidermis and $T_{sur} = T_{air}$ on the lower. With this, the solutions Supplemental Text S1, Equations 1.17 and 1.18 for the upper nontranspiring domain could be evaluated at $L_d$ and the solutions Supplemental Text S1, Equations 1.23 and 1.24 for the transpiring domain at $L_b$, to find four equations with six unknowns: $T_{Ld}$, $\psi_{Ld}$, $T_o$, $\psi_o$, $T_{Lb}$, and $\psi_{Lb}$. With $E_d = 0$ for no transpiration from the upper surface and the source water potential ($\psi_r$) given, $\psi_o$ was found from global molecular conservation (Supplemental Text S1, Equation 1.36), and global energy conservation (Supplemental Text S1, Equation 1.35) provided the required constraints on $T_{Ld}$, $T_{Lb}$, and $\psi_{Lb}$ that closed the system of equations for the five remaining unknowns. We then solved the system using the FindRoot command of Mathematica 8 (Wolfram Research). As before, for the first iteration of the solution, the physical properties $\overline{\lambda}, \chi_\psi, \chi_T, cD_v$ were evaluated at $T_{air}$, and the vascular scaling factor $\varsigma$ was defined by Equation 25 and leaf hydraulic conductivity by Equation 26. For the second iteration, these properties were recalculated at $T_o$ and $\psi_o$, and $\varsigma$ was reestimated using the effective nonisothermal $k_l$ from Equation 27. Finally, a check of the neglected enthalpy transport terms (due to molecular fluxes through a temperature field) described in Supplemental Text S1 verified that they were indeed negligible relative to the retained latent and conductive fluxes (Supplemental Text S4).

## Sunflower Cold-Mirror Experiment Model

As not all model inputs were available from the data of Pieruschka et al. (2010), some parameters had to be estimated from previous reports or assumed (Table III). Specifically, the original data contained no information on hydraulic parameters or variables, so values had to be assumed, and thus the absolute water potentials reported are arbitrary values; a constant water potential of −0.2 MPa was assumed to exist at the petiole/stem junction. As sunflower (*Helianthus annuus*) is amphistomatous, the solution was sought for two transpiring domains, with total $g_s$ partitioned arbitrarily but in a manner consistent with a larger flux from the abaxial side (Foster, 1986). Radiative boundary conditions were set for a laboratory with all surfaces at $T_{air}$, the partitioning of $SR$ between the upper and lower domain was set at 90% and 10%, respectively, and the thermal conductivity of the cells was assumed to be 0.2 W $mol^{-1}$ $K^{-1}$.

After solution of the model for the cold-mirror initial state, $SR = 160$, we then constructed equations to describe the linear response of $g_s$ to small perturbations in water potential (Supplemental Text S5) when at approximately 80% of maximum aperture, based on the shape of responses described by Franks and Farquhar (2007). We then changed $SR$ to its full-mirror value of 200 and resolved the model based on environmental inputs with both $g_s$ and surface temperatures as variables. To capture the effect of the temperature compensation described by Pieruschka et al. (2010), ambient air temperature in the model was adjusted iteratively to bring lower epidermal temperature to within 0.01°C of its initial at $SR = 160$.

The explore the effect of air fraction and upper and lower domain symmetry on the magnitude of stomatal opening at the higher radiation level, we modeled the cold-mirror experiment for three different total air fractions (0.3, 0.5, and 0.7), employing the assumption of Pieruschka et al. (2010) that stomata change aperture to hold epidermal water potential constant (Supplemental Text S6).

## Condensing Leaf and Evaporative Flux Meter Models

To construct a condensing leaf model (Supplemental Text S7), we started with the exposed leaf solution for an oak leaf and then varied the air fraction in each domain and external humidity as guided by Equation 17 to bring the lower epidermis into a condensing state, with final values of 0.75 in the spongy and 0.2 in the palisade domains and relative humidity of 85%. Other leaf parameters were left unchanged. As we were not concerned with the absolute values of the water potentials, and because the temperature gradients are nonlinear in the condensing limit, we neglected the vascular scaling factor. In addition, to capture the effect of a whole-plant canopy responding to environmental forcing, we allowed the stem water potential $\psi_r$ to vary by assuming a soil water reservoir potential and per leaf whole plant conductance, such that:

$$\psi_r = \psi_g + \psi_s - \frac{E}{K_{rs}} \tag{28}$$

where $\psi_g$ is the standing gravitational potential and $K_{rs}$ is the effective conductance of the root and stem to the modeled leaf. To allow $g_s$ to respond in a manner consistent with steady-state hydraulic feedbacks, an arbitrary model based on the form of aperture and turgor relations described by Franks and Farquhar (2007) was adopted:

$$g_s = g_{max}\left(1 - \exp\left[\frac{-5.2\times10^6 - \psi_{Lb}}{1.5\times10^6}\right]\right) \tag{29}$$

where $g_{max}$ was estimated as 0.36 mol $m^{-2}$ $s^{-1}$ based on data from oak trees at Harvard Forest (Williams et al., 1996). For the evaporative flux meter model, we set $\psi_r$ to a small but nonzero value to avoid division by zero errors, with an air fraction of 0.3, and adopted radiative boundary conditions suitable for a laboratory of $T_{sur} = T_{air}$ (Supplemental Text S8).

## Supplemental Data

The following materials are available in the online version of this article.

**Supplemental Figure S1.** Oak leaf humidity and energy perturbations.

**Supplemental Figure S2.** Sunflower air fraction and stomatal symmetry variations.

**Supplemental Text S1.** Model description and overview of derivation.

**Supplemental Text S2.** Detailed model derivation and appendices.

**Supplemental Text S3.** Oak model code.

**Supplemental Text S4.** Evaluation of enthalpy convection terms code.

**Supplemental Text S5.** Sunflower model code.

**Supplemental Text S6.** Sunflower epidermal potential set-point model code.

**Supplemental Text S7.** Condensing oak-like leaf model code.

**Supplemental Text S8.** Evaporative flux meter model code.

Received January 20, 2014; accepted February 21, 2014; published February 26, 2014.

## LITERATURE CITED

**Bird RB, Stewart WE, Lightfoot EN** (1960) Transport Phenomena. John Wiley & Sons, New York

**Bowen IS** (1926) The ratio of heat losses by conduction and by evaporation from any wet surface. Phys Rev **27:** 779–787

**Boyce CK, Brodribb TJ, Feild TS, Zwieniecki MA** (2009) Angiosperm leaf evolution was physiologically and environmentally transformative. Proc Royal Soc B **276:** 1771–1776

**Boyer JS** (1969) Free-energy transfer in plants. Science **163:** 1219–1220

**Boyer JS** (1985) Water transport. Annu Rev Plant Physiol **36:** 473–516

**Brodribb TJ, Feild TS, Jordan GJ** (2007) Leaf maximum photosynthetic rates and venation are linked by hydraulics. Plant Physiol **144:** 1890–1898

**Brodribb TJ, Feild TS, Sack L** (2010) Viewing leaf structure and evolution from a hydraulic perspective. Functional Plant Biol **37:** 488–498

**Brodribb TJ, Holbrook NM** (2006) Declining hydraulic efficiency as transpiring leaves desiccate: two types of response. Plant Cell Environ **29:** 2205–2215

**Buckley TN** (2005) The control of stomata by water balance. New Phytol **168:** 275–292

**Buckley TN, Mott KA** (2013) Modeling stomatal conductance in response to environmental factors. Plant Cell Environ **36:** 1691–1699

**Buckley TN, Sack L, Gilbert ME** (2011) The role of bundle sheath extensions and life form in stomatal responses to leaf water status. Plant Physiol **156:** 962–973

**Byott GS** (1976) Leaf air space systems in C3 and C4 species. New Phytol **76:** 295–299

**Byott GS, Sheriff DW** (1976) Water movement into and through *Tradescantia virginiana* (L.) leaves. II. Liquid flow pathways and evaporating sites. J Exp Bot **27:** 634–639

**Campbell GS, Norman JM** (1998) An Introduction to Environmental Biophysics. Springer-Verlag, New York

**Cernusak LA, Kahmen A** (2013) The multifaceted relationship between leaf water $^{18}O$ enrichment and transpiration rate. Plant Cell Environ **36:** 1239–1241

**Chen IT, Pharkya A, Stroock AD** (2014) Analysis of superheated loop heat pipes exploiting nanoporous wick membranes. AIChE J **60:** 762–777

**Crank J** (1957) The Mathematics of Diffusion. Oxford University Press, New York

**Deen WM** (1998) Analysis of Transport Phenomena. Oxford University Press, New York

**Dengler NG** (1980) Comparative histological basis of sun and shade leaf dimorphism in *Helianthus annuus*. Can J Bot **58:** 717–730

**DeVries DA** (1958) The simultaneous transfer of heat and moisture in porous media. Trans Am Geophys Union **39:** 909–916

**Farquhar GD, Lloyd J, Taylor JA, Flanagan LB, Syvertsen JP, Hubick KT, Wong SC, Ehleringer JR** (1993) Vegetation effects on the isotope composition of oxygen in atmospheric $CO_2$. Nature **363:** 439–443

**Foster JR, Smith WK** (1986) Influence of stomatal distribution on transpiration in low wind environments. Plant Cell Environ **9:** 751–759

**Franks PJ, Farquhar GD** (2007) The mechanical diversity of stomata and its significance in gas-exchange control. Plant Physiol **143:** 78–87

**Gillon JS, Yakir D** (2000) Naturally low carbonic anhydrase activity in $C_4$ and $C_3$ plants limits discrimination against $C^{18}OO$ during photosynthesis. Plant Cell Environ **23:** 903–915

**Kenzo T, Ichie T, Watanabe Y, Hiromi T** (2007) Ecological distribution of homobaric and heterobaric leaves in tree species of Malaysian lowland tropical rainforest. Am J Bot **94:** 764–775

**Kittel C, Kroemer H** (1980) Thermal Physics. Freeman, New York

**Knipling EB** (1970) Physical and physiological basis for the reflectance of visible and near-infrared radiation from vegetation. Remote Sens Environ **1:** 155–159

**Kramer PJ, Boyer JS** (1995) Water Relations of Plants and Soils. Academic Press, San Diego

**Lambers H, Chapins FS, Pons TL** (1998) Plant Physiological Ecology. Springer, New York

**Meidner H** (1976) Water vapour loss from a physical model of a substomatal cavity. J Exp Bot **27:** 691–694

**Molz FJ, Ferrier JM** (1982) Mathematical treatment of water movement in plant cells and tissues: a review. Plant Cell Environ **5:** 191–206

**Mott KA** (2007) Leaf hydraulic conductivity and stomatal responses to humidity in amphistomatous leaves. Plant Cell Environ **30:** 1444–1449

**Nobel PS** (2005) Physicochemical and Environmental Plant Physiology. Elsevier Academic Press, Burlington, MA

**Peak D, Mott KA** (2011) A new, vapour-phase mechanism for stomatal responses to humidity and temperature. Plant Cell Environ **34:** 162–178

**Pesacreta TC, Hasenstein KH** (1999) The internal cuticle of Cirsium horridulum (Asteraceae) leaves. Am J Bot **86:** 923–928

**Philip JR** (1966) Plant water relations: some physical aspects. Annu Rev Plant Physiol **17:** 245–268

**Philip JR, DeVries DA** (1957) Moisture movement in porous materials under temperature gradients. Trans Am Geophys Union **38:** 222–232

**Pickard WF** (1981) The ascent of sap in plants. Prog Biophys Mol Biol **37:** 181–229

**Pickard WF** (1982) Why is the substomatal chamber as large as it is? Plant Physiol **69:** 971–974

**Pieruschka R, Huber G, Berry JA** (2010) Control of transpiration by radiation. Proc Natl Acad Sci USA **107:** 13372–13377

**Raupach MR** (2001) Combination theory and equilibrium evaporation. Q J R Meteorol Soc **127:** 1149–1181

**Rockwell FE** (2010) Leaf water transport. PhD thesis. Harvard University, Cambridge, MA

**Rockwell FE, Holbrook NM, Stroock AD** (2014a) Leaf hydraulics. I. Scaling transport properties from single cells to tissues. J Theor Biol **340:** 251–266

**Rockwell FE, Holbrook NM, Stroock AD** (2014b) Leaf hydraulics. II. Vascularized tissues. J Theor Biol **340:** 267–284

**Rockwell FE, Holbrook NM, Zwieniecki MA** (2011) Hydraulic conductivity of red oak (*Quercus rubra* L.) leaf tissue does not respond to light. Plant Cell Environ **34:** 565–579

**Sack L, Melcher PJ, Zwieniecki MA, Holbrook NM** (2002) The hydraulic conductance of the angiosperm leaf lamina: a comparison of three measurement methods. J Exp Bot **53:** 2177–2184

**Song X, Barbour MM, Farquhar GD, Vann DR, Helliker BR** (2013) Transpiration rate relates to within- and across-species variations in effective path length in a leaf water model of oxygen isotope enrichment. Plant Cell Environ **36:** 1338–1351

**Tanton TW, Crowdy SH** (1972) Water pathways in higher plants. III. The transpiration stream within leaves. J Exp Bot **23:** 619–625

**Tyree MT, Yianoulis P** (1980) The site of water evaporation from substomatal cavities, liquid path resistances, and hydroactive stomatal closure. Ann Bot (Lond) **46:** 175–193

**Vogel S** (1983) The lateral thermal conductivity of leaves. Can J Bot **62:** 741–744

**Vogelmann TC, Evans JR** (2002) Profiles of light absorption and chlorophyll within spinach leaves from chlorophyll fluorescence. Plant Cell Environ **25:** 1313–1323

**Whitaker S** (1977) Simultaneous heat, mass, and momentum transfer in porous media: a theory of drying. *In* JP Hartnett, TF Irvine, eds, Advances in Heat Transfer, Vol 13. Academic Press, New York, pp 119–203

**Williams M, Rastetter EB, Fernandes DN, Goulden ML, Wofsy SC, Shaver GR, Melillo JM, Munger JW, Fan SM, Nadelhoffer KJ** (1996) Modeling the soil-plant-atmosphere continuum in a *Quercus-Acer* stand at Harvard Forest: the regulation of stomatal conductance by light, nitrogen and soil/plant hydraulic properties. Plant Cell Environ **19:** 911–927

**Wylie RB** (1952) The bundle sheath extension in leaves of dicotyledons. Am J Bot **39:** 645–651

**Yianoulis P, Tyree MT** (1984) A model to investigate the effect of evaporative cooling on the pattern of evaporation in sub-stomatal cavities. Ann Bot (Lond) **53:** 189–206